Key Points:

- Symbiont photosynthesis raises pH in the microenvironment of planktic foraminifera
- Foraminifera species-specific offsets in boron proxies are the same in laboratory culture and in the natural oceanic environment
- Symbiont photosynthesis alone does not explain species-specific boron proxy offsets in planktic foraminifera

Correspondence to:

B. Hönisch,
hoenisch@ldeo.columbia.edu

Symbiont Photosynthesis and Its Effect on Boron Proxies in Planktic Foraminifera

Bärbel Hönisch[1,2] , **Carina R. Fish[1,3,4]** , **Samuel R. Phelps[1,2,5]** , **Laura L. Haynes[1,2,6]** , **Kelsey Dyez[1,7]** , **Kate Holland[8]** , **Jennifer Fehrenbacher[9]** , **Katherine A. Allen[1,2,10]** , **Stephen M. Eggins[8]** , and **Joaquim I. Goes[1]**

[1]Lamont-Doherty Earth Observatory, Columbia University, Palisades, NY, USA, [2]Department of Earth and Environmental Sciences, Columbia University, New York, NY, USA, [3]Now at Bodega Marine Laboratory, University of California Davis, Bodega Bay, CA, USA, [4]Now at Department of Earth and Physical Sciences, University of California Davis, Davis, CA, USA, [5]Now at Department of Earth and Planetary Sciences, Harvard University, Cambridge, MA, USA, [6]Now at Vassar College, Poughkeepsie, NY, USA, [7]Now at Department of Earth and Environmental Sciences, University of Michigan, Ann Arbor, MI, USA, [8]Research School of Earth Sciences, The Australian National University, Canberra, NSW, Australia, [9]College of Earth, Ocean, and Atmospheric Sciences, Oregon State University, Corvallis, OR, USA, [10]Now at School of Earth and Climate Sciences, University of Maine, Orono, ME, USA

Abstract Boron proxies in the calcium carbonate shells of planktic foraminifera are sensitive to seawater acidity, but B/Ca ratios and isotopic composition (i.e., $\delta^{11}B$) recorded by different foraminifer species grown under identical environmental conditions differ significantly and systematically. Specifically, *Globigerinoides ruber* displays higher B/Ca and $\delta^{11}B$ than *Trilobatus sacculifer* and *Orbulina universa*. It has been hypothesized that these differences are caused by species-specific rates of symbiont photosynthesis and habitat depth with greater symbiont photosynthesis elevating the microenvironmental pH of *G. ruber* relative to *T. sacculifer* and *O. universa*. Here we test this hypothesis by applying fast repetition rate fluorometry (FRRF), Chlorophyll *a* quantification, and symbiont counts in laboratory grown specimens of *G. ruber* (pink), *T. sacculifer* and *O. universa* to study species-specific differences in symbiont photochemical quantum efficiencies. In addition, we report B/Ca shell profiles measured by laser ablation on the same specimens previously monitored by FRRF, and $\delta^{11}B$ data of discrete populations of all three species grown under high and low light conditions in the laboratory. While the light experiments document that symbiont photosynthesis elevates pH and/or $\delta^{11}B$ in the calcifying microenvironment of all three foraminifer species, the FRRF, Chl. *a* and symbiont abundance data are relatively uniform among the three species and do not scale consistently with intrashell B/Ca, or with observed species-specific offsets in B/Ca or $\delta^{11}B$. Implications of these findings for foraminiferal physiology and biomineralization processes are discussed.

1. Introduction

Elemental and isotopic compositions of fossil foraminifer shells provide important proxies for paleoenvironmental growth conditions and are widely applied in paleoceanographic research. Foraminiferal boron isotopic composition ($\delta^{11}B$) and boron-to-calcium ratios (B/Ca) are closely related to seawater pH. This is because boron in seawater is primarily present in the form of boric acid and borate ions, and the relative abundance and isotopic composition of these chemical species depends on seawater pH (Dickson, 1990b; Klochko et al., 2006). Because the $\delta^{11}B$ of marine carbonates falls close to the $\delta^{11}B$ of dissolved borate in seawater, Vengosh et al. (1991) and Hemming and Hanson (1992) suggested that the charged borate ion is preferentially incorporated into biogenic calcite. This hypothesis has subsequently been tested in sediment and laboratory studies, which confirmed that $\delta^{11}B$ and B/Ca of planktic foraminifera shells increase with seawater-pH (Allen et al., 2011, 2012; Henehan et al., 2013; Sanyal et al., 1996, 2001; Yu et al., 2007).

Although the aqueous systematics of boron proxies are relatively straightforward, physiological processes such as respiration, calcification and symbiont photosynthesis can alter the abundance and speciation of dissolved carbon and boron in the microenvironment of a foraminifer. For instance, CO_2 consumption by symbiont photosynthesis increases pH in the microenvironment of planktic foraminifers by up to 0.5 units, whereas respiration in the dark releases CO_2 and thereby decreases pH by up to 0.4 units near the shell surface (Jørgensen et al., 1985; Köhler-Rink & Kühl, 2005; Rink et al., 1998). These physiological processes

translate to the $\delta^{11}B$ and B/Ca compositions of cultured, symbiont-bearing foraminifera which are higher when specimens are grown in the light compared to specimens grown in near darkness (Haynes et al., 2017; Hönisch et al., 2003). Similarly, symbiont-barren species record relatively lower $\delta^{11}B$ and B/Ca values than their symbiont-bearing relatives (Foster, 2008; Henehan et al., 2016; Hönisch et al., 2003, 2019; Osborne et al., 2020; Yu et al., 2007, 2013). These observations are consistent with the hypothesis that foraminiferal respiration and calcification lower pH in the microenvironment of symbiont-barren species, and that of symbiont-bearing species in the dark (Foster, 2008; Henehan et al., 2016; Hönisch et al., 2003; Zeebe et al., 2003). Micro-scale variation (banding) in B/Ca across shell walls of the symbiont-bearing *O. universa* grown in the laboratory, where light was varied on a 12-hr light/dark cycle, suggests that even diurnal variations in light availability affect boron incorporation into planktic foraminifer shells (Allen et al., 2011; Holland et al., 2017).

Sediment and plankton net studies provide further evidence for physiological processes playing an important role in these proxies' systematics. For instance, the $\delta^{11}B$ of symbiont-bearing planktic foraminifera shells systematically increases with shell size (Henehan et al., 2013, 2016; Hönisch & Hemming, 2004). This observation has been interpreted to reflect a shallower growth environment for larger specimens with higher light levels and greater symbiont photosynthetic activity (Hönisch & Hemming, 2004), or an increasing ratio of photosynthesis-to-respiration in larger specimens (Henehan et al., 2013). A relationship between size and photosynthesis (or the photosynthesis/respiration ratio) has been shown experimentally, where the final shell size of *T. sacculifer* was found to be directly related to the light levels specimens were exposed to (Caron et al., 1981; Spero & Lea, 1993). The importance of symbiosis to the final size of *T. sacculifer* was also clearly demonstrated in an experiment that compared shell sizes in specimens that had active symbionts with specimens whose symbionts had been chemically eliminated (Bé et al., 1982). In this experiment, final shell sizes in specimens without symbionts were greatly reduced relative to specimens whose symbiont population was reinstated after chemical elimination. Furthermore, some studies suggest that species-specific boron proxy offsets are primarily related to the depth habitat of different foraminifer species, with species recording lower B/Ca and $\delta^{11}B$ values potentially living deeper in the water column where lower light levels decrease the photosynthesis/respiration ratio (e.g., Foster, 2008; Henehan et al., 2016). Finally, Babila et al. (2014) studied B/Ca in the symbiont-bearing *G. ruber* from sediment traps off Bermuda, and found seasonal variations that correlate most closely with variations in light intensity and hence symbiont photosynthesis.

In summary, multiple lines of evidence indicate physiological processes affect boron proxy incorporation into planktic foraminifera shells, with symbiont photosynthesis often suggested as the dominant control. Moreover, distinct offsets also occur between the boron proxy compositions of different foraminifera species that harbor the same species of photosynthetic symbiont and experience identical environmental conditions in the laboratory, including light levels, culture medium chemistry and temperature (Figure 1). Because the laboratory conditions were the same for all species, explaining these geochemical offsets requires a more nuanced investigation of the physiological processes specific to each foraminifer species. For instance, do symbiont density (Spero & Parker, 1985) or species-specific chemical modification of the calcifying fluid and differences in biomineralization pathways such as those observed by Bentov et al. (2009), Erez (2003), and de Nooijer et al. (2014) play additional roles? Respiration has been shown to increase with temperature and shell size within both *G. ruber* and *O. universa* (Lombard et al., 2009), but interspecies differences are uncertain due to the small number of specimens analyzed (Figure S1). Furthermore, an intermediate-sized *T. sacculifer* specimen analyzed by Jørgensen et al. (1985) yielded much higher photosynthesis and respiration rates than projected from the *G. ruber* and *O. universa* comparison, leaving hypotheses based on the photosynthesis/respiration ratio intriguing but inconclusive at this time.

Understanding the nature and extent of biological controls on proxy relationships is important for paleoreconstructions, as physiological modifications of the foraminiferal growth environment could potentially alter proxy relationships and thus lead to erroneous data interpretations. Here we use controlled laboratory cultures to test the effects of symbiont photosynthetic activity on boron proxy offsets observed between *G. ruber* (pink), *T. sacculifer* and *O. universa*. Following the observations described above, and based on the specific boron proxy offsets displayed in Figure 1, we test whether symbiont photosynthesis is greatest in *G.*
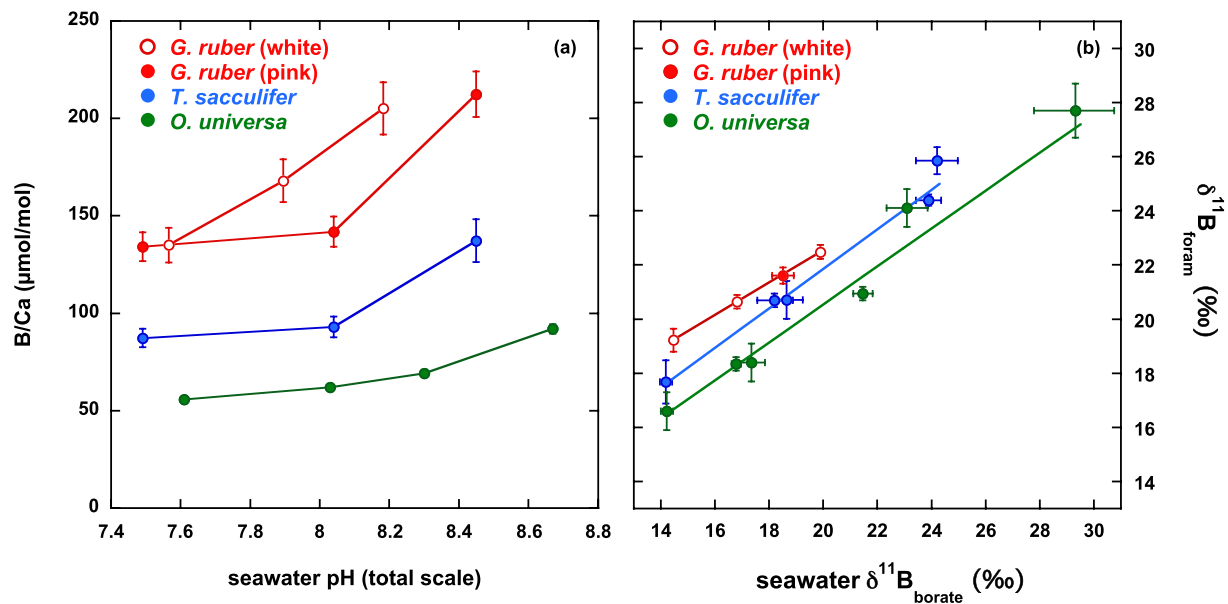
Figure 1. Published laboratory calibrations of B/Ca and δ^{11}B in planktic foraminifera. (a) B/Ca of *G. ruber* (white) (Henehan et al., 2013), *G. ruber* (pink) and *T. sacculifer* (Allen et al., 2012), and *O. universa* (Allen et al., 2011) increases with pH, but *O. universa* records the lowest B/Ca values and *G. ruber* the highest. (b) Similar patterns and offsets are observed in δ^{11}B when all data are normalized to the same analytical technique, see Text S1 for details. Foraminiferal δ^{11}B data are shown versus δ^{11}B of aqueous borate, which increases with pH analogous to panel (a). B/Ca error bars reflect the long-term 1sd of a consistency standard, δ^{11}B error bars are 2se and 2sd for TIMS and MC-ICP-MS analyses, respectively.

ruber (pink), followed by *T. sacculifer* and *O. universa*. Images of living specimens of these foraminifera and their symbiont associations are shown in Figure S2.

Our study takes advantage of the fact that the three foraminifer species studied herein harbor the same species of dinoflagellate symbiont, *Pelagodinium béii* (Shaked & de Vargas, 2006; Siano et al., 2010; Spero, 1987), thus eliminating possible symbiont-species effects. To shed light on different aspects of the symbiont-host relationship and shell geochemical signatures, we present a suite of experiments, including observations of species-specific and ontogenetic variations in symbiont photosynthesis with fast repetition rate fluorometry (FRRF), symbiont counts, Chl. *a* concentrations, laser ablation analysis of B/Ca incorporation in shells previously monitored by FRRF, and bulk shell δ^{11}B and B/Ca analyses of foraminifera populations grown in the light and in near darkness.

2. Materials and Methods

2.1. Foraminifer Collection and General Culture Conditions

The majority of the live foraminifer specimens studied herein were collected approximately eight nautical miles off the coast of La Parguera, Lajas, Puerto Rico (17°58′12″N, 67°2′42″W) during March–May 2015. Individual specimens were hand-collected by SCUBA divers from approximately 5 m water depth. Following collection, foraminifer species were identified under a stereomicroscope and measured on width and length across the final and penultimate (i.e., F to F-1, respectively) and penultimate and antepenultimate (i.e., F-1 to F-2, respectively) chambers using an inverted microscope. Specimens were then transferred into 120-mL soda lime glass jars filled with 0.8-μm filtered natural seawater from the collection site, sealed with Parafilm®, capped with tight fitting lids and placed into temperature- (26°C) and light-controlled culture tanks. The culture tanks were topped with LUMILUX skywhite T5 (24W) fluorescent lamps with an enhanced blue spectrum, adjusted to ~300 μmol photons m^{-2} s^{-1} and operated on a 12 h light:12 h dark cycle (i.e., lights were on from 7 a.m. to 7 p.m.). These light levels exceed the saturation light intensities of the *O. universa* and *T. sacculifer* symbiont associations (Jørgensen et al., 1985; Spero & Parker, 1985). For *G. ruber*, the light saturation concentration has not yet been quantified but given that all three foraminifer species host the same symbiont species, *P. béii*, we assume that its light saturation levels should be similar to *T. sacculifer*
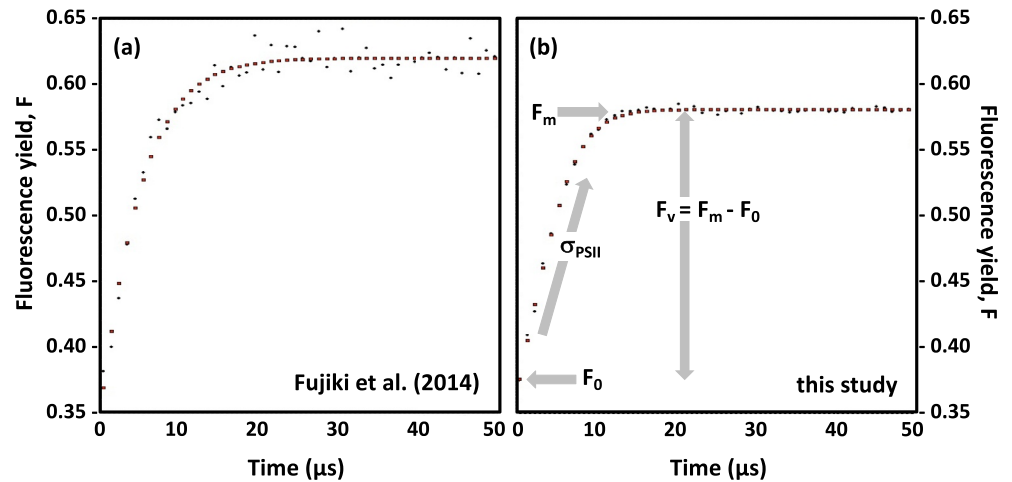
Figure 2. Fluorescence yield of the foraminiferal symbiont association (black dots), biophysical model fit (red dots) after Kolber et al. (1998) and depiction of fluorescence parameters defined in the text. In comparison to the original method of (a) Fujiki et al. (2014), our protocol (b) Reduces scatter and variance but also systematically decreases F_m and increases σ_{PSII}.

and *O. universa*. Experimental light levels were monitored every 10 days using a Biospherical Instruments QSL 2200 light meter, temperature was recorded every 5 min with a TidbiT® temperature logger, and salinity was measured with an Orion Star Thermo Scientific conductivity meter (salinity resolution = ±0.1‰). For comparison, sea surface temperature at the dive site rose from 26°C in March to 28°C in April, and sea surface salinity increased from 35.9 to 36.5‰ over the same period. Cultured foraminifera were fed every other day with a 1-day-old brine shrimp nauplius (*Artemia salina*), starting with the day after collection.

2.2. Foraminifer Sampling Strategy

Because pigment analyses and symbiont counts each require individual foraminifers to be terminated, we studied our FRRF specimens in two groups. In the first group, hereafter referred to as *ontogenetic specimens*, foraminifers were monitored in the laboratory from the day of collection until gametogenesis. These specimens were observed daily for chamber formation (i.e., growth), the presence or absence of spines and symbionts, the expansion of cytoplasm in newly-formed chambers, and FRRF-derived photo-physiological properties (Figure 2). FRRF parameters include maximum fluorescence (i.e., when the light-harvesting complexes of the symbionts are saturated; F_m), minimum fluorescence of dark conditioned specimens (F_0), variable fluorescence ($F_v = F_m - F_0$), photochemical quantum efficiencies (F_v/F_m) and functional absorption cross sections of photosystem II (σ_{PSII}) (Falkowski et al., 2004; Kolber et al., 1998). We monitored a total of four *T. sacculifer*, four *G. ruber* (pink), and one *O. universa* specimens throughout their ontogeny in the laboratory. Symbiont abundance and pigment concentrations could not be measured on these specimens.

Specimens constituting the *ocean group* were analyzed and terminated the same day they were collected. Foraminifers in this group were measured on their longest shell dimension and photo-physiological properties by FRRF immediately after collection. Fifty-nine of these specimens were analyzed for Chl. *a*, most of them individually, but for eight samples we pooled 2–4 similarly sized specimens to ensure that the pigment concentration was within the detection limits of our analytical technique. To preserve specimens for later pigment analysis at the Lamont-Doherty Earth Observatory (LDEO), they were transferred to individual 0.7 μm Whatman GF/F glass microfiber filters (25 mm diameter) immediately after FRRF analysis. Filters were then folded, placed into Bio Plas polypropylene histocapsules and frozen immediately at −80°C. At the end of the field season these samples were transported frozen to LDEO, where they were again stored at −80°C until analysis.

Several additional specimens were analyzed for symbiont abundance. Similar to other foraminifera, these specimens were identified to the species level and their shell size was measured on the longest dimension before further processing for symbiont counts. In addition to three *T. sacculifer*, ten *G. ruber* (pink) and three *O. universa* specimens from Puerto Rico, this assessment also includes data from twenty-four *O. universa*

specimens collected on Santa Catalina Island (California) in July/August 2013. Sea surface temperature and salinity at the time and site of collection in California were 19.2°C and 33.2‰, respectively.

Finally, light experiments for boron proxy analysis were performed across two culture seasons in Puerto Rico. Specifically, high light (HL) experiments with *O. universa* and *T. sacculifer* were performed in March–May 2010, whereas high and low light (LL) experiments with *G. ruber* (pink) and LL experiments with *O. universa* and *T. sacculifer* were completed in March–May 2015. Specimens from the *G. ruber* (pink) LL experiment were also measured for trace elements including B/Ca. Salinity and alkalinity of seawater collected at the dive site were somewhat lower in 2010 ($S = 35.5$, TA = 2,340 µmol kg^{-1}) than in 2015 ($S = 36.6$, TA = 2,370 µmol kg^{-1}), but ambient pH$_{TS}$ ~ 8.05 and temperature were the same within measurement error. The same experimental and analytical techniques were applied, so that the data collected from these two field seasons are directly comparable. Similar to foraminifera collected and cultured for FRRF, foraminifera for the light experiments were collected by SCUBA diving, identified under a stereomicroscope, measured for their largest dimension, and then placed into jars of filtered natural seawater collected at the dive site. Foraminifera were then transferred into culture tanks, fed and monitored in the same way as for other experiments described above. HL experiments were performed at saturating light levels (~300 µmol photons m^{-2} s^{-1}) and LL experiments at photosynthesis-limiting light levels of ~20 µmol photons m^{-2} s^{-1} (Spero & Parker, 1985). The experiments ended upon gametogenesis; empty shells were then removed from the culture jars, rinsed in MilliQ water and archived for later analysis at LDEO (boron isotopes) and Rutgers University (B/Ca). Seawater-pH (on the NBS scale) and alkalinity were measured at the beginning and end of each experiment using a Metrohm 809 open cell autotitrator calibrated with NBS standards, and pH$_{NBS}$ was converted to the total scale using CO2SYS (version 2.3, Pierrot et al., 2006), K$_1$ and K$_2$ from Lueker et al. (2000), K$_{SO_4}$ from Dickson (1990a), and the seawater total boron concentration from Lee et al. (2010). Culture conditions are reported in Data Set S1.

2.3. Fast Repetition Rate Fluorometry

For FRRF measurements, specimens had to be briefly removed from their culture jars. Measurements followed the method of Fujiki et al. (2014) and were performed in two custom-built quartz glass cuvettes with raised platforms to position the foraminifera in the center of the FRRF measurement window. Cuvette cavity diameters were 7–8 mm, so that foraminifers and a small amount of seawater could be transferred with minimal spine damage and disruption of the symbiont swarm. FRRF measurements were performed no earlier than 3 h after the incubator lights were turned on, as Spero and Parker (1985) reported maximum photosynthetic rates of these symbiont associations are only achieved at and after that time. Using glass pipettes with an inner diameter of ~5 mm, live foraminifer specimens were individually transferred into cuvettes, and incubated for 30 min in the dark to ensure that the reaction centers were open during FRRF measurements. During analysis, each specimen was measured four times with the cuvette rotated by 90° to avoid any bias introduced by variations in the position of the foraminifer in the cuvette. The resulting data of the 4 analyses were then averaged. After each FRRF measurement, specimens were returned to their culture jars and culture tanks.

The FRRF instrument used for our measurements (Diving Flash, Kimoto Electric Co. Ltd) is identical to the model used by Fujiki et al. (2014) and Takagi et al. (2016). Typical fluorescence induction curves, showing transient changes in fluorescence yield over time are shown in Figure 2. Fujiki et al. (2014) applied blue light excitation flashlets of 30 mmol quanta m^{-2}s^{-1} for 2 µs durations, followed by 2 µs breaks. Their protocol is composed of 50 acquisitions with 50 excitation flashlets each for a total of 2,500 flashlets. To reduce the scatter and variance from the biophysical model fit to the data (Figure 2a), we modified these acquisition settings (Figure 2b) by subdividing each acquisition into 50 sequences with 50 excitation flashlets per sequence, but reduced the number of acquisitions to 15. These modifications increased the total number of flashlets from 2,500 to 37,500. Light quality and intensity, cuvette rotation, replication and data averaging were identical to the original protocol of Fujiki et al. (2014).

2.4. Pigment Analysis

Chlorophyll *a* concentrations were determined fluorometrically at LDEO, using a Turner Designs Trilogy model No. 7200-040 (Holm-Hansen & Riemann, 1978). The fluorometer was pre-calibrated with a Sigma

Chemicals analytical Chl. *a* standard. To extract the pigments, the filters containing the foraminifera and symbionts were submerged in 3 mL of 90% acetone in disposable borosilicate glass culture tubes (12 × 75 mm). The tubes were capped and transferred into a −20°C freezer for 24 h to ensure complete extraction of Chl. *a* (Holm-Hansen & Riemann, 1978; JGOFS-protocols, 1996). Filters were then carefully removed from the test tube with tweezers and discarded. The acetone extracts were then analyzed fluorometrically before and after acidification with two drops of 1.2 M HCl to correct Chl. *a* concentrations for phaeopigments. Where 2–4 specimens were pooled for analysis, data were subsequently divided by the number of specimens per sample to yield the pigment concentration in nanograms (ng) per specimen (Data Set S4).

2.5. Symbiont Counts

Symbiont counts in adult specimens were undertaken as follows: On the day of collection, individual live foraminifer specimens were transferred into 2-mL plastic vials using glass pipettes. In contrast to Spero and Parker (1985), who crushed their specimens between glass slides, dispersed the cytoplasm containing Lugol-stained symbionts between the slides and counted the entire symbiont population of each specimen, we first decalcified individual foraminifer shells and subsequently dispersed their symbionts in a defined volume. Specifically, after transfer of a specimen into the vial, we siphoned off all seawater using a Pasteur pipette and replaced it with 100 µl of a 0.1 M saline EDTA solution. The vial was then capped and the calcareous foraminifer shell dissolved within 30 min. Using a micropipettor, 15 µl of Lugol's solution were then added to the vial to stain starch molecules in the symbionts. For 5–10 min, the solution was repeatedly taken up and expelled back into the vial with the micropipettor in order to release the symbionts from the foraminiferal cytoplasm and ensure their homogenous suspension within the solution. Once well mixed, two 15-µl aliquots were pipetted onto two glass slides and covered with glass coverslips. Because Lugol stain fades with time and the solution evaporates, symbionts were counted immediately in each aliquot using an inverted microscope at 200x magnification. The counts of the two slides were averaged and extrapolated to the full volume of the solution.

2.6. Boron Isotope Analysis

Cultured foraminifera typically add between one and three new chambers under controlled laboratory conditions. To isolate these chambers from the portion of the shell that was grown in the open ocean prior to collection, we compared each specimen's shell dimension at the time of collection with its dimension after gametogenesis and amputated culture-grown chambers with a medical scalpel under a microscope. Amputations were only required for *G. ruber* and *T. sacculifer*, as adult *O. universa* secrete a spherical chamber that comprises ∼95% of the entire shell weight (Lea et al., 1995). This small contribution of the juvenile shell is negligible compared to the large geochemical differences between experimental treatments (Figure 1 and data collected herein, see results). Species-specific amputated chambers or spherical final shells were then pooled and oxidatively cleaned following previously established protocols for cultured foraminifera with a relatively high concentration of organic matter (e.g., Russell et al., 2004). Cleaned samples were then dissolved in 2N ultrapure HCl and from this solution, replicate aliquots of 1 ng boron each were loaded onto outgassed Rhenium filaments and mounted into the Triton TIMS at LDEO. Data acquisition followed the procedures detailed in Foster et al. (2013). Results are reported relative to the NBS SRM 951 boric acid standard in Data Set S1, with standard errors calculated as $2SE = 2*standard\ deviation/\sqrt{N}$, where N is the number of replicate analyses that meet the acceptance criteria for boron isotope analyses by N-TIMS. These internal uncertainties are compared to the external long-term uncertainty of an equal number of repeat measurements of an in-house standard of NBS SRM 951 precipitated in $CaCO_3$ matrix (vaterite), and the larger of the two uncertainties is reported.

2.7. Solution Analysis of Trace Element Ratios

Amputated chambers of *G. ruber* (pink) from the LL experiment were cleaned following the same oxidative procedure used for $\delta^{11}B$. Prior to analysis, the sample was dissolved in 0.065 N HNO_3. The solution was then measured for B/Ca on an Element-XR ICP-MS at Rutgers University. B/Ca ratios were determined using a single in-house gravimetrically spiked standard (B/Ca = 178.2 µmol/mol) following the methodology de-

scribed by Rosenthal et al. (1999) and Babila et al. (2014). Repeat measurements of an in-house consistency standard of 160 μmol/mol B/Ca were made at the beginning and end of the run; the RSD of these analyses was 0.8% ($N = 2$), which was applied to the single B/Ca data point to estimate analytical uncertainty. For conservative comparison to the ambient *G. ruber* (pink) data of Allen et al. (2012), we apply their reported 5.2% long-term RSD to estimate the uncertainty on our new B/Ca data point.

To quantify matrix effects, a (Ca) matrix of 1.5–8 mM was run and used to make corrections at the end of the run (Rosenthal et al., 1999). A linear matrix correction was applied based on the measured B/Ca of these in-house matrix standards; on average the matrix correction changed the B/Ca ratio by 0.46%.

2.8. Laser Ablation Analysis of Trace Element Ratios in Individual Shell Walls

The shells of five *ontogenetic* foraminifer specimens (two *G. ruber* (pink), two *T. sacculifer* and one *O. universa*) were analyzed by laser ablation inductively coupled plasma mass spectrometry (LA-ICP-MS) to produce high resolution geochemical profiles. The foraminifer shells had previously been monitored by FRRF over the duration of their ontogeny in the laboratory, so that direct comparisons can be made between the FR-RF-derived photo-physiological parameters and the geochemical signals measured by laser ablation. Laser ablation was performed at the Research School of Earth Sciences at The Australian National University following established procedures (e.g., Eggins et al., 2004). To prepare shells for analysis, they were oxidatively cleaned by immersion in a 50:50 solution of 30% H_2O_2 and 0.1 N NaOH in a water bath at 55 °C for ~10 min, and then rinsed and sonicated three times in ultra-pure Milli-Q (>18 MΩ-cm). Whole specimens of *G. ruber* and *T. sacculifer* were mounted on carbon tape for ablation from the outside of the shell wall through to the inside. For these two species, the three youngest chambers were analyzed for all specimens, that is, the final (F), penultimate (F-1) and antepenultimate (F-2) chambers. In the case of *O. universa*, the terminal spherical chamber is large and without any internal support structures, so ablation from the outside to the inside tends to break the shell before complete profiles can be collected. To prevent this, we cracked the chamber with a scalpel. Shell fragments were cleaned and then mounted on double-sided carbon tape for ablation
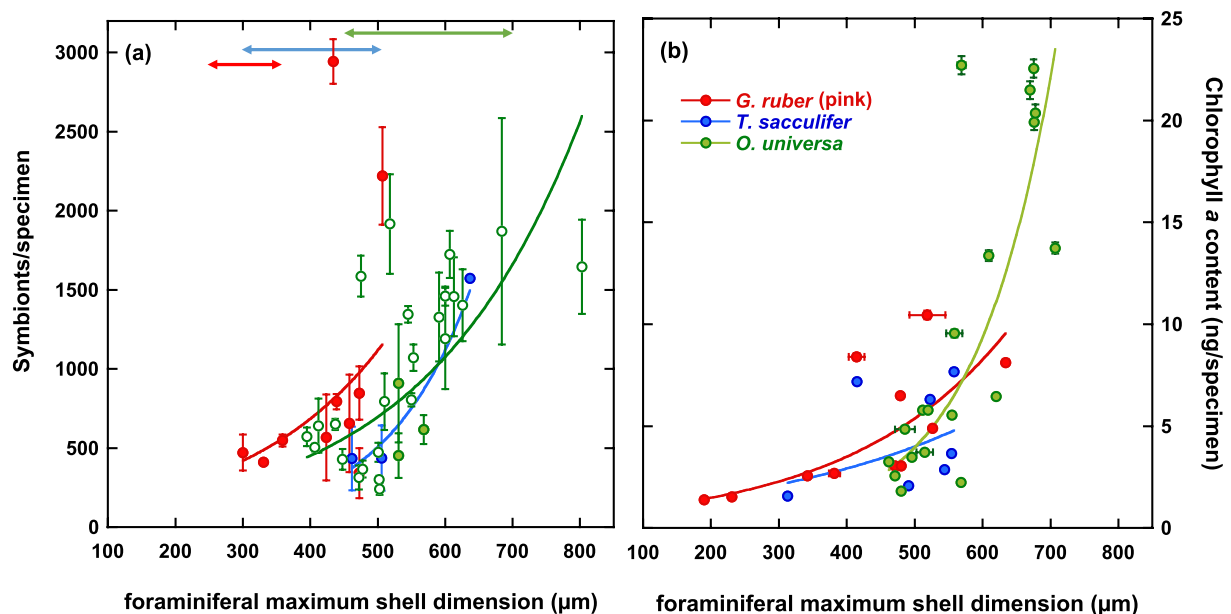

Figure 3. (a) Symbiont counts and (b) Chl. *a* content were analyzed on separate groups of specimens and increase with foraminiferal shell dimension. Symbols and exponential fits (solid lines) are color-coded, with red = *G. ruber* (pink), blue = *T. sacculifer* and green = *O. universa*. The colored double arrows at the top of the graph indicate the shell size range typically used for geochemical analysis in paleoceanographic (*G. ruber* (pink): 250–355 μm e.g., Arbuszewski et al., 2010; Martínez-Botí et al., 2015), *T. sacculifer*: 300–500 μm (e.g., Dyez et al., 2018; Seki et al., 2010) and culture studies (450–700 μm, *O. universa*, e.g., this study). Closed symbols display data collected on Isla Magueyes in Puerto Rico, open green symbols data collected on Catalina in California. Symbiont error bars in panel (a) reflect 1sd of duplicate analyses, maximum shell dimension uncertainty in panels (a) and (b) is estimated as ±5 μm. In panel (b) maximum shell dimension uncertainty for 2–4 pooled foraminifer specimens is reported as their size range. Chlorophyll *a* uncertainty is ±2%.

from the inside of the shell wall through to the outside. Only the final spherical chamber was analyzed by laser ablation for this species.

The 193-nm ArF Excimer laser was pulsed at a repetition rate of 2 Hz, with a 72 μm square spot size and energy density (fluence) of approximately 2 J/cm². Each laser pulse is estimated to remove ∼0.1 μm of shell material (Eggins et al., 2003). Ablated material is carried via a helium-argon gas mixture from the HelEx cell to a Varian 820 Quadrupole ICP-MS. Selected isotopes (^{7}Li, ^{10}B, ^{11}B, ^{24}Mg, ^{25}Mg, ^{27}Al, ^{43}Ca, ^{44}Ca, ^{88}Sr, and ^{238}U) were measured in rapid peak hopping mode for between 10–30 ms in each mass spectrometer cycle depending on their isotopic abundance.

The SRM NIST610 glass was used for external calibration, to assess the ablation yield and to enable drift correction. Data reduction followed established procedures (Longerich et al., 1996), which involves despiking by removing data points that are >7σ of their immediate neighboring measurements, then subtracting the mean background, which is measured with the laser off before and after sets of 5–10 unknown analyses. Each element analyzed was normalized to the measured internal isotope standard intensities of ^{43}Ca. The data integration window excludes any signal that showed evidence of organic matter contamination (diagnosed by elevated Mg) on the inner or outer surface of the shell. Two to three repeat profile measurements on the same chamber of a specimen were aligned using AnalySeries (v2.0.8; Paillard et al., 1996), interpolated, and combined to calculate the averaged profiles. The profile alignment was made using Mg/Ca signals, which typically show more pronounced cyclic variations than B/Ca. Similarly, B/Ca values were interpolated to match each time step of the reference profile and then averaged to establish the combined profile (see Data Set S5). A 5-point running mean was applied to each averaged profile.

3. Results

3.1. FRRF Method Comparison

We compared the original Fujiki et al. (2014) and our revised analytical protocols throughout the field season on several foraminifer specimens from the *ontogenetic* and *ocean groups* (Figure S3). We find F_0 data are nearly identical using either protocol but F_m data are consistently lower than data obtained with the original protocol. Similarly, F_v/F_m values are consistently lower for our protocol, while our σ_{PSII} values are slightly elevated. Crossplots of the individual results and linear fits are shown in Figures S3a–S3d and Equations S1–S4. The observed differences between the two protocols are independent of the studied foraminifer species.

To ascertain that the observed data differences are not introduced by the sequential application of both analytical protocols to each specimen, we tested whether they are a function of which method was applied first. To do this, we switched the order of the two protocols during the analysis of one *ontogenetic G. ruber* specimen on consecutive days. The resulting data are consistent regardless of which protocol was applied first (Figures S3e–S3h). All other data collected in this study were collected with our revised protocol first, and from here on we only display and interpret data collected with our protocol.

3.2. Symbiont Counts

Figure 3a and Data Set S2 present the symbiont abundances of individual specimens of the three foraminifera species studied herein, each analyzed over a range of shell sizes. Unfortunately, experimental constraints did not allow us to dedicate more than three *T. sacculifer* specimens to this analysis, but the trend of these three data points generally agrees with the better constrained *G. ruber* (pink) and *O. universa* data sets. The number
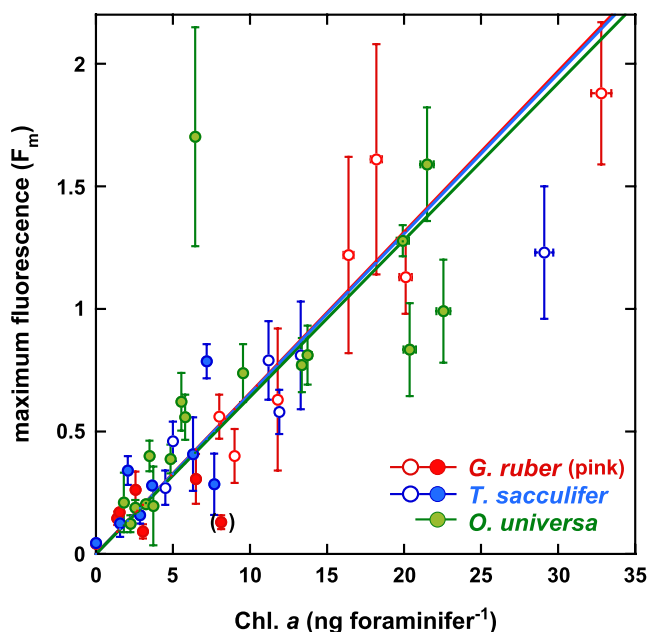
Figure 4. Chlorophyll *a* increases with F_m. Solid symbols reflect data collected for this study, and open symbols data from Fujiki et al. (2014) whose F_m values were adjusted to our fast repetition rate flourometry analytical protocol using Equation S2. Lines display linear least squares weighted fits forced through the origin. F_m error bars reflect 1sd of four replicate analyses, with the cuvette rotated after each analysis. Chlorophyll *a* uncertainty is ±2%. The data point in parentheses stems from a very large *G. ruber* specimen (634 μm max. shell dimension) that we assume must have been near gametogenesis (see also Figure 6a) and therefore does not reflect normal ontogenetic F_m values.

of symbionts per foraminifer generally increases with size for each of the three species, where estimated symbiont counts range from ~300 to 3,000 symbionts per host for *G. ruber* (pink), ~400–1,600 symbionts per host for *T. sacculifer*, and ~250–1,900 symbionts per host for *O. universa* (see also Figure S2d for a photograph of an adult *O. universa* with many more symbionts than the juvenile *O. universa* shown in Figure S2c). In contrast to an earlier study, all *O. universa* specimens analyzed herein were adults with spherical chambers, and the symbiont numbers are significantly lower than extrapolated from the juvenile specimens counted with the different techniques in the earlier study (i.e., 3,200–23,300 symbionts/adult specimen, Spero & Parker, 1985). Exponential regressions weighted by the uncertainty in symbiont counts yield:

$$N_{\text{symb}(G.ruber)} = 51.61(\pm 91.4)e^{0.007(\pm 0.004)*l_{\max}}, R^2 = 0.25, P = 0.010 \qquad N = 10, \tag{1}$$

$$N_{\text{symb}(O.universa)} = 84.16(\pm 44.68)e^{0.004(\pm 0.001)*l_{\max}}, R^2 = 0.35, P < 0.001 \qquad N = 27, \tag{2}$$

where n_{symb} is the number of symbionts and $l_{\max}$ is the maximum shell dimension in μm. We do not report a regression for *T. sacculifer*, as the data set includes only three data points.

The analyzed *G. ruber* (pink) specimens range in maximum shell dimension from 300 to 507 μm, and within this size range, *G. ruber* (pink) tends to host relatively more symbionts than *O. universa* and *T. sacculifer*. However, when considering the gametogenic shell dimensions typically analyzed in culture studies and paleoceanographic reconstructions (see color arrows in Figure 3a), *O. universa* hosts up to three times as many symbionts as *G. ruber* (pink). The symbiont abundance in *T. sacculifer* tends to range intermediate in this comparison, although the small sample size for this species prevents a firm assessment.

3.3. Chlorophyll *a* Content and FRRF Parameters in the *Ocean Group*

The Chl. *a* content of the symbiont population associated with the *G. ruber* (pink) specimens studied herein ranges from 1.4–10.5 ng foraminifer⁻¹, from 1.6–7.7 ng foraminifer⁻¹ in *T. sacculifer*, and from 3.3–22.7 ng foraminifer⁻¹ in *O. universa* (Figure 4b, Data Set S3). Chlorophyll *a* content increases with shell size (Figure 3b):

$$\text{Chl. } a_{G.ruber}(\text{ng}) = 0.73(\pm 0.44)e^{0.004(\pm 0.001)*l_{\max}}, R^2 = 0.68, P < 0.001 \qquad N = 10, \tag{3}$$

$$\text{Chl. } a_{T.sacculifer}(\text{ng}) = 0.78(\pm 1.24)e^{0.003(\pm 0.003)*l_{\max}}, R^2 = 0.31, P = 0.010 \qquad N = 7, \tag{4}$$

$$\text{Chl.} a_{O.universa}(\text{ng}) = 0.17(\pm 0.18)e^{0.007(\pm 0.002)*l_{\max}}, R^2 = 0.60, P < 0.001 \qquad N = 19, \tag{5}$$

where Chl. *a* is the mass (ng) per specimen and $l_{\max}$ is the maximum shell dimension in μm.

In addition, and in agreement with previous observations on *G. ruber* and *T. sacculifer* by Fujiki et al. (2014), a greater Chl. *a* content is associated with greater F_m in all three species (Figure 4). Linear least squares fits forced through the origin, weighted by the 1sd uncertainty in F_m and including the data of Fujiki et al. (2014), yield:

$$F_{mG.ruber} = 0.066(\pm 0.001) * Chl. a \quad N = 13, \tag{6}$$

$$F_{mT.sacculifer} = 0.065(\pm 0.001) * Chl. a \quad N = 14, \tag{7}$$

$$F_{mO.universa} = 0.064(\pm 0.001) * Chl. a \quad N = 17, \tag{8}$$

These slopes are the same within their linear least squares errors (i.e., ±0.001).

Figure 5 displays FRRF data collected from the *ocean group*, that is, those foraminifera that were analyzed immediately after collection and then terminated for Chl. *a* sampling (Figures 3b and 4). Similar to Chl. *a* (Figure 3b), F_m also increases with shell size (Figure 5a). Because *O. universa* tends to produce the largest volume shells of the three species and harbors the most symbionts with highest Chl. *a* concentrations (Figure 3), it yields the highest F_m (0.12–1.70), whereas *G. ruber* (pink) and *T. sacculifer*
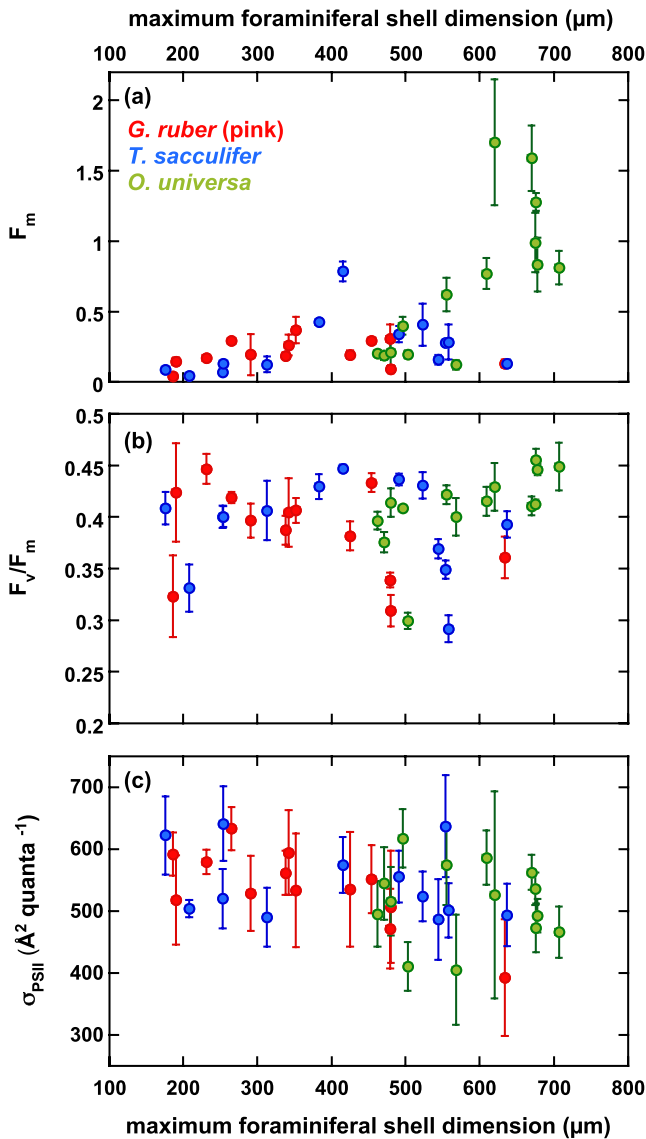
Figure 5. (a) F_m, (b) F_v/F_m and (c) σ_{PSII} values of foraminifer specimens from the *ocean group*. Symbols are color-coded for each species. Error bars are 1sd for all parameters.

yield relatively smaller F_m values (0.04–0.37 and 0.05–0.078, respectively). F_v/F_m (Figure 5b) and σ_{PSII} (Figure 5c) values are similar for all three species (F_v/F_m = 0.39 ± 0.04, 0.39 ± 0.05, and 0.41 ± 0.04, and σ_{PSII} = 538 ± 61, 546 ± 59, and 516 ± 65 for *G. ruber*, *T. sacculifer*, and *O. universa*, respectively) and display a slightly decreasing trend with larger shell sizes.

3.4. *Ontogenetic* Trends in FRRF Parameters

The FRRF parameters F_m, F_v/F_m, and σ_{PSII} for the nine specimens observed throughout their ontogeny are shown in Figures 6 and 7. Daily visual observations of *ontogenetic* specimens included the shells' maximum dimension, which increases stepwise when foraminifera grow new chambers. Toward the end of a specimen's life cycle, the golden color of the symbionts disappears as the symbionts are expelled or digested (Bé et al., 1983), and the color of particularly long-lived specimens (e.g., *G. ruber* [pink] specimen #615, Figures 6 and 7d) may even turn gray or white as the symbionts' peridinin pigment is replaced by colorless gametes during meiosis. Observations ended with each specimen's gametogenesis, although two specimens (Figures 6, 7a and 7d) had to be terminated prematurely.

Similar to the trends in the *ocean group* (Figure 5a), we observed increasing F_m with shell size, but our *ontogenetic* observations reveal that F_m usually peaks 2–4 days prior to gametogenesis (Figure 6, Data Set S4). This pattern is most pronounced in *T. sacculifer*, which shows two days of declining F_m values in Figures 6a, 6e and 6h five-day decline in Figure 6f, and in Figure 6g just one day before gametogenesis. These *T. sacculifer* specimens grew in culture for 13–16 days, with Figure 6f displaying a near zero F_m value on this specimen's last day in culture. Similarly, *G. ruber* (pink) specimens are shown in Figures 6c and 6d display a clear F_m maximum, although F_m in the specimen in Figure 6c dropped abruptly before gametogenesis, whereas the specimen in Figure 6d lived unusually long and eventually had to be terminated before gametogenesis because the field season ended. This specimen's F_m decrease occurred gradually but did not drop to near zero over the observation period. The two remaining *G. ruber* (pink) specimens (Figures 6a and 6b) showed little F_m variability over their ontogeny, but the specimen in Figure 6a also had to be terminated before gametogenesis, such that the ontogenetic observations are incomplete and we cannot say whether it would or would not have displayed the pre-gametogenic F_m decrease. The only analyzed *O. universa* specimen showed a 3-day F_m decline before gametogenesis. The observed pre-gametogenic F_m decreases suggest a decline in symbiont biomass in all three species prior to gametogenesis. Maximum values reach F_m = 0.50 ± 0.27 in *G. ruber* (pink, n = 4), F_m = 0.84 ± 0.28 in *T. sacculifer* (n = 4), and F_m = 1.20 in *O. universa* (n = 1). Similar to the ocean group (Figure 5a), the F_m data for *G. ruber* and *T. sacculifer* are the same within overlapping 1sd errors.

F_v/F_m (Figure 7) is generally much less variable than F_m (Figure 6); a slight F_v/F_m decline is observed in all specimens two to three days prior to gametogenesis (Figure 7). Species averages before the pre-gametogenic decline are the same within error, F_v/F_m = 0.36 ± 0.03 for *O. universa*, F_v/F_m = 0.37 ± 0.08 for *T. sacculifer*, and F_v/F_m = 0.40 ± 0.05 for *G. ruber* (pink).

None of the foraminifer species studied herein display a clear ontogenetic trend in σ_{PSII} (Figure 7). The average value for the four *G. ruber* (pink) specimens is 509 ± 71 Å² quanta⁻¹, 525 ± 68 Å² quanta⁻¹ for *T.*
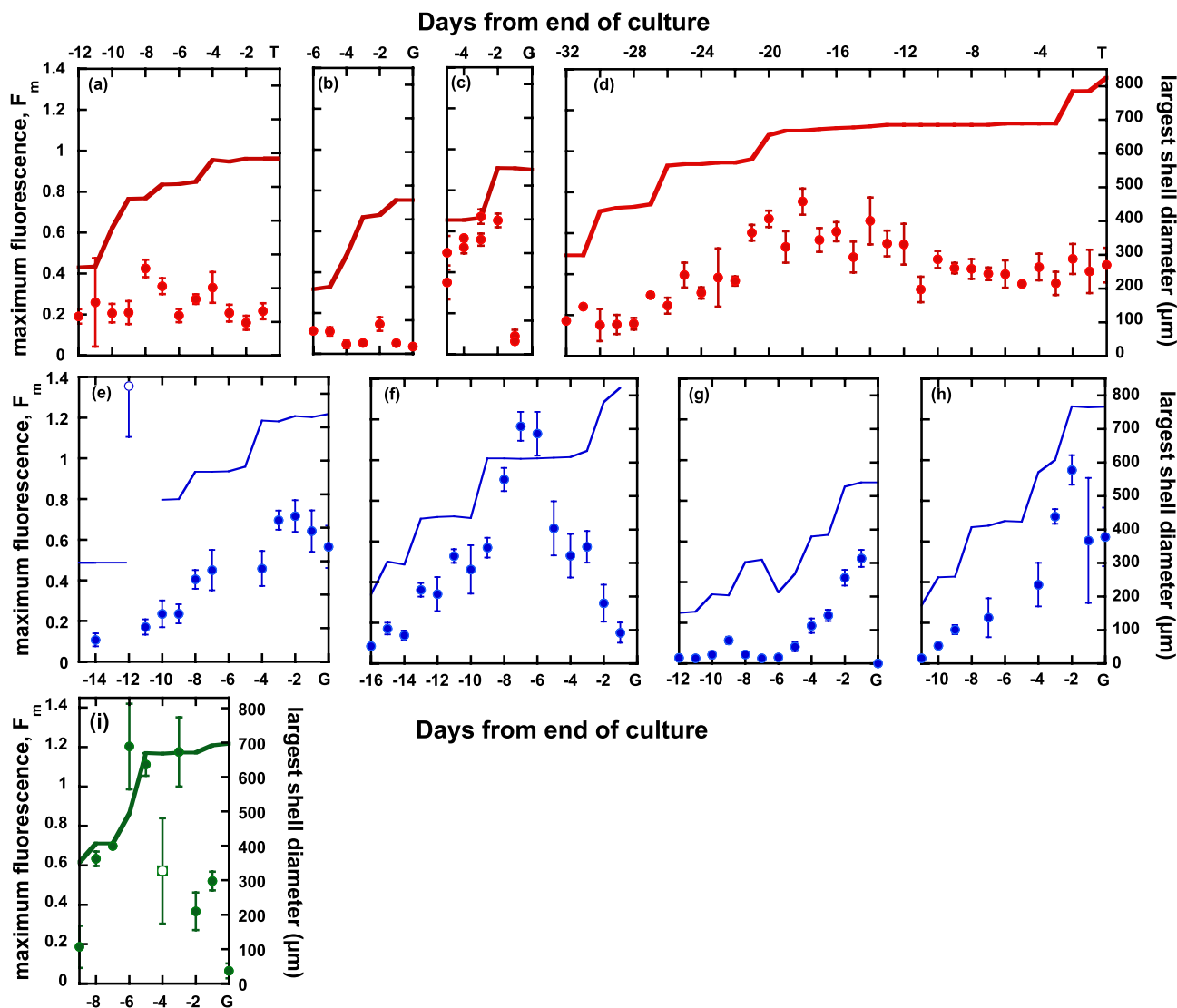
Figure 6. Nine *ontogenetic* specimens' shell growth (solid lines) and F_m yield (solid symbols) from day of collection to gametogenesis (indicated by letter *G* on *x*-axes). (a–d) display *G. ruber* (pink) (red symbols and lines), (e–h) *T. sacculifer* (blue symbols and lines), and (i) *O. universa* (green symbols and line). Data uncertainties have been determined as for Figure 4. Open symbols in panels (e) and (i) are considered outliers, as indicated by their F_m deviation from that of the previous and following day, and in panel (i) by the poor reproducibility of this value between replicate measurements. Letter *T* at the top of panels (a) and (d) indicates specimens terminated before natural gametogenesis.

sacculifer ($n = 4$), and 564 ± 54 Å^2 quanta^{-1} for *O. universa* ($n = 1$). These values are the same within error for all three species.

3.5. Light Effects on Geochemical Proxies: Bulk Shell Boron Isotopic and B/Ca Composition

Boron isotope data for foraminifera grown under HL or LL conditions are summarized in Data Set S1 and shown in Figure 8. Data are shown relative to species-specific laboratory calibrations for *O. universa* (Hönisch et al., 2009; Sanyal et al., 1996), *T. sacculifer* (Dyez et al., 2018; Sanyal et al., 2001), and *G. ruber* (white, Henehan et al., 2013, shifted by $+1.1‰$ to make the MC-ICP-MS calibration compatible with our N-TIMS analyses, see Text S1).

Similar to previously published culture studies (Figure 1; Dyez et al., 2018; Henehan et al., 2013; Hönisch et al., 2009; Sanyal et al., 2001, 1996) and sediment coretop observations (Foster, 2008; Henehan et al., 2016), *G. ruber* (pink, Figure 8a) records higher δ^{11}B than *T. sacculifer* (Figure 8b) and *O. universa* (Figure 8c) at

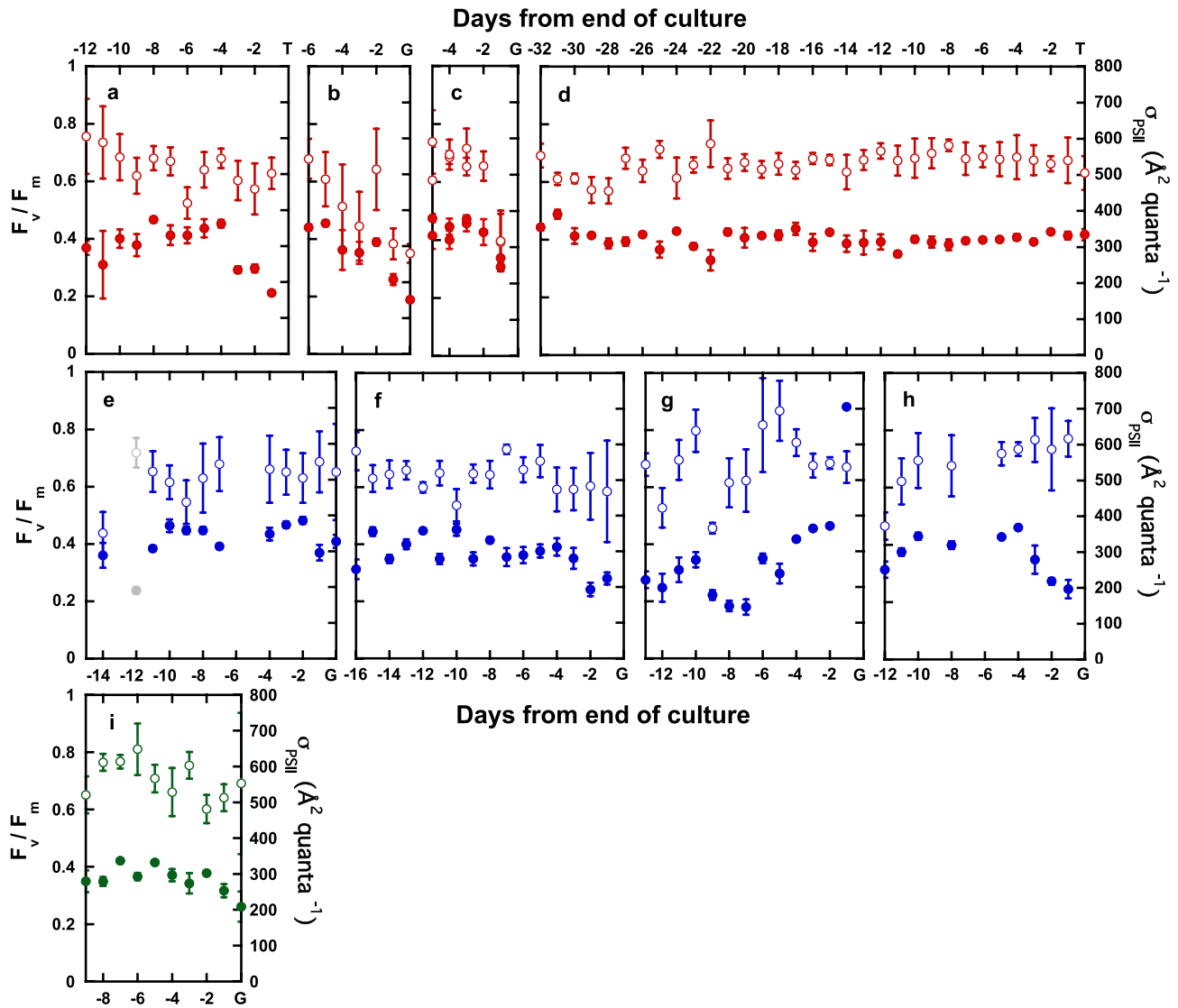**Figure 7.** Nine *ontogenetic* specimens' trends in F_v/F_m (solid symbols) and σ_{PSII} (open symbols) from the day of collection to gametogenesis. Gray symbols in panel (e) are considered outliers as in Figure 6e. For species, error bars, and notes, see Figure 6.

the same $\delta^{11}B_{borate}$. All three species also record at least 2‰ higher $\delta^{11}B$ when grown under HL compared to LL; the exact HL-LL offsets are reported in Figure 8. The magnitude of the HL-LL offset in *O. universa* depends on the HL data point to which the LL value is compared. The HL samples of *T. sacculifer* and *O. universa* were both grown during the 2010 culture season in Puerto Rico, whereas the LL samples of these two species were grown during the 2015 Puerto Rico culture season, along with the HL and LL samples of *G. ruber*. While the HL *T. sacculifer* data point falls within error of the published $\delta^{11}B$-pH calibration of this species (solid line in Figure 8b; Dyez et al., 2018; Sanyal et al., 2001), the HL *O. universa* data point is 1.3‰ higher than that of published calibrations for this species, which were produced from foraminifera grown on Catalina (dashed line in Figure 8c; Hönisch et al., 2009; Sanyal et al., 1996). A possible reason for this difference is discussed further below. At this point, we conclude that the HL-LL $\delta^{11}B$ offset is either consistently ~2‰ for all three species, or possibly as large as 3.2‰ for *O. universa*.

In addition to new $\delta^{11}B$ data, we also report a new LL B/Ca data point for *G. ruber* (pink) of 115 ± 1 µmol/mol, which compares to 141 ± 7 µmol/mol in HL conditions (Allen et al., 2012) (Figure 9). For *O. universa*, HL and LL experiments had previously been published from Puerto Rico and Catalina. Whereas the *O. universa* Catalina experiments revealed no B/Ca difference between the two light conditions, the Puerto Rico
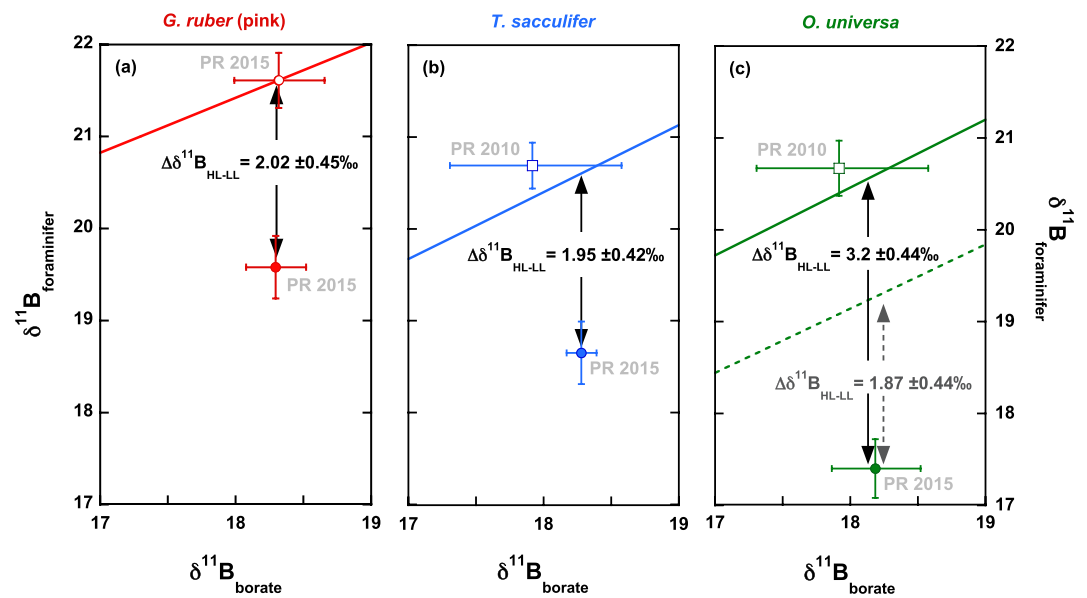
Figure 8. Boron isotopic composition of foraminifera grown under high light (HL) (open symbols) and low light (LL) conditions (filled symbols). Open squares in panels (b) and (c) indicate samples grown during the 2010 culture season, all other data are from samples grown in 2015 (gray labels indicate culture season). Lines are published laboratory culture calibrations for each species (see text and Figure 1 for details). The dashed line in panel (c) displays the Catalina culture data of Sanyal et al. (1996) and Hönisch et al. (2009), the solid line represents the same calibration shifted by +1.3‰ to pass through the Puerto Rico HL point. The $\delta^{11}B$ HL-LL difference for each species is indicated by the vertical arrows. In (c) the dashed arrow indicates the $\Delta\delta^{11}B_{HL-LL}$ offset relative to the published Catalina calibration, and the solid arrow the $\Delta\delta^{11}B_{HL-LL}$ offset relative to the +1.3‰-shifted calibration. See Section 4 for details.

LL *O. universa* sample recorded B/Ca = 58 ± 4 μmol/mol and the HL experiment B/Ca = 66 ± 4 μmol/mol (Allen et al., 2011; Haynes et al., 2017).

3.6. Light Effects on Geochemical Proxies: B/Ca Shell Profiles

Laser ablation profiles from chambers that were precipitated in the laboratory while the foraminifera was monitored by FRRF are shown in Figure 10. Laser ablation data (Figures 10k–10t) are presented with the shell's inside on the left-hand side and outside on the right-hand side of each graph and have been tied to FRRF data via the position of the primary organic sheet (POS) of the ablated chamber. In the laser ablation profile, the POS can be identified by the respective minimum in Mg/Ca of each ablated chamber (Eggins et al., 2004; Holland et al., 2017; Sadekov et al., 2005; Spero et al., 2015); in the FRRF data, the POS of each ablated chamber is indicated by the stepwise increase in maximum shell dimension (Figures 10a–10e, Data Set S5). The calcite shell is thicker on the outer side of the POS than on the inner side, which means the outer shell calcite provides a higher-resolution record of ontogenetic geochemical variations. To allow maximum overlap between FRRF and laser ablation data, Figure 10 presents the F-1 chamber for *G. ruber* specimen 1475 (Figure 10, column 1), the F-2 chambers for *G. ruber* specimen 615 (Figure 10, column 2) and both *T. sacculifer* specimens (Figure 10, columns 3 and 4), and the spherical F-chamber for *O. universa* (Figure 10, column 5). The end of the laser profile coincides with the last day of FRRF measurements. It should be noted that this alignment is only quasi-temporal, as we know the exact day and time of FRRF measurement and the day of chamber formation, but we do not know the time scale of the shell thickening process between the production of consecutive chambers. Consequently, if minima and maxima in FRRF and geochemical data correspond, they may not be perfectly aligned and this should be considered when comparing these data.

Laser ablation profiles of B/Ca ratios are overall higher in *G. ruber* (pink) and lower in *O. universa*, and the absolute ratios are generally comparable between solution chemistry and laser ablation techniques (Figures 1a, 9 and 10p–10t). However, both intra-specimen and inter-species variability are large in B/Ca and
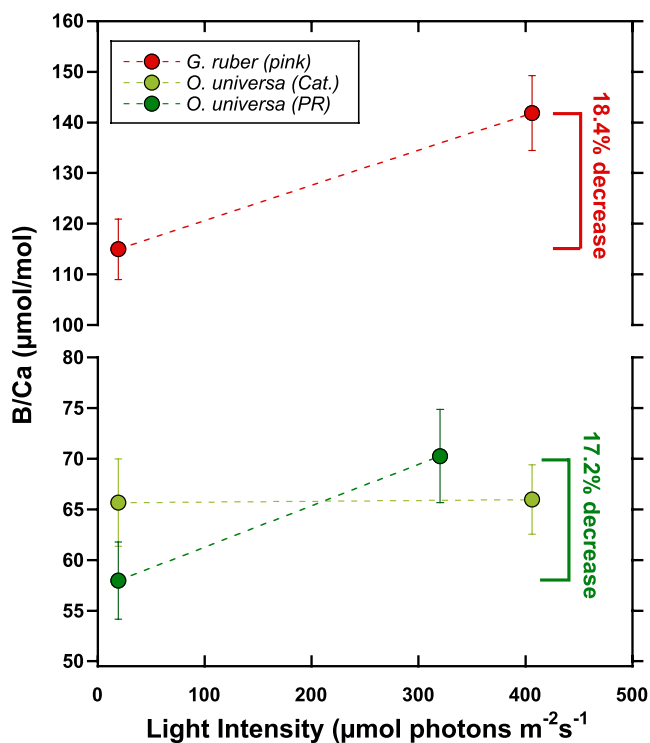
Figure 9. B/Ca ratios of *G. ruber* (pink) and *O. universa* grown under high light (HL) and low light (LL) conditions in the laboratory. Catalina *O. universa* specimens do not show a B/Ca difference between HL and LL conditions (dark green symbols), but Puerto Rico *O. universa* (light green symbols) and *G. ruber* (pink) B/Ca is 17%–18% lower in LL-specimens. Dashed horizontal lines trace the B/Ca value of LL data points to the light intensity of the HL experiments. Vertical error bars represent analytical RSD.

Mg/Ca despite culturing at equivalent and constant environmental conditions (Figures 10p–10t). Systematic B/Ca banding in these specimens is somewhat masked by the wide B/Ca scale that is applied in Figure 10 so that we can better compare absolute values. Each specimen's B/Ca ratio increases with distance in either direction from the POS, suggesting elevated B incorporation during shell thickening rather than during chamber initialization. The rate of B/Ca elevation generally decreases preceding gametogenesis, except for *G. ruber* specimen #615 because it was terminated early, and *T. sacculifer* specimen #128 shows a B/Ca slope reversal. The same pattern is not visible at the very inner shell surface, which may be due to the lower spatial resolution of calcification inwards of the POS (see also Data Set S5 for a few chamber surface laser ablation data that have been omitted from Figure 10 due to axes scaling). B/Ca and Mg/Ca patterns show some similarities, but shifts in B/Ca appear to be delayed relative to Mg/Ca.

Whether the maxima and minima of B/Ca and F_m coincide temporally is difficult to ascertain without absolute time control on the laser ablation profiles. Qualitatively, it appears that when F_m and F_v/F_m begin to decrease prior to gametogenesis, the rates of change of B/Ca and Mg/Ca decline (e.g., Figures 10r–10t) and in some cases invert (e.g., Figures 10m–10o). F_v/F_m and σ_{PSII} show little variability across specimens and species, but F_m appears to vary inversely with B/Ca. For instance, *O. universa* displays the highest F_m values (Figures 4 and 10e) but lowest B/Ca (Figure 10t). Similarly, maximum F_m values for *G. ruber* are lower (Figures 4, 10a and 10b) than observed for *T. sacculifer* (Figures 4, 10c and 10d) or *O. universa*, but B/Ca ratios in *G. ruber* (Figures 10p and 10q) are generally higher than in *T. sacculifer* (Figure 10s) and *O. universa*. It is difficult to generalize from these observations because *T. sacculifer* specimen #128 displays intermediate F_m (Figure 10c) but elevated B/Ca (Figure 10r), whereas specimen #640 displays the highest F_m (Figure 10d) but relatively low B/Ca values (Figure 10s) similar to those of *O. universa* (Figure 10t).

4. Discussion

Our experiments and observations were designed to test whether the higher B/Ca and boron isotope ratios of *G. ruber* compared to *T. sacculifer* and *O. universa* (Figure 1) are due to species-specific photosynthetic pH elevation in the foraminiferal microenvironment. If correct, we would expect greater symbiont photosynthetic activity in *G. ruber* > *T. sacculifer* > *O. universa*. In the following, we will separately evaluate symbiont abundance, Chl. *a* concentration, light-induced fluorescence and experimental B/Ca and δ^{11}B data with respect to this hypothesis.

4.1. Symbiont Abundance and Chl. *a* Concentration

We find several lines of evidence suggesting greater photosynthesis in larger foraminifera specimens. First, the number of symbionts per specimen and their cumulative Chl. *a* concentration increases with the maximum shell dimension of the foraminifera studied herein (Figure 3). Second, and similar to earlier observations by Fujiki et al. (2014), F_m increases with the Chl. *a* concentration (Figure 4), indicating greater symbiont biomass in larger specimens that harbor more symbionts with more Chl. *a*. These observations are consistent with a previous study of symbiont abundance on juvenile (i.e., pre-sphere) *O. universa* by Spero and Parker (1985) and Chl. *a* concentrations measured in a range of foraminifer species by Fujiki et al. (2014) and Takagi et al. (2016, 2019).

Our inter-species comparison (Figure 3a) shows that relatively large *G. ruber* (pink) specimens (i.e., 400–500 μm) may harbor more symbionts with higher Chl. *a* concentration than *T. sacculifer* and *O. universa*
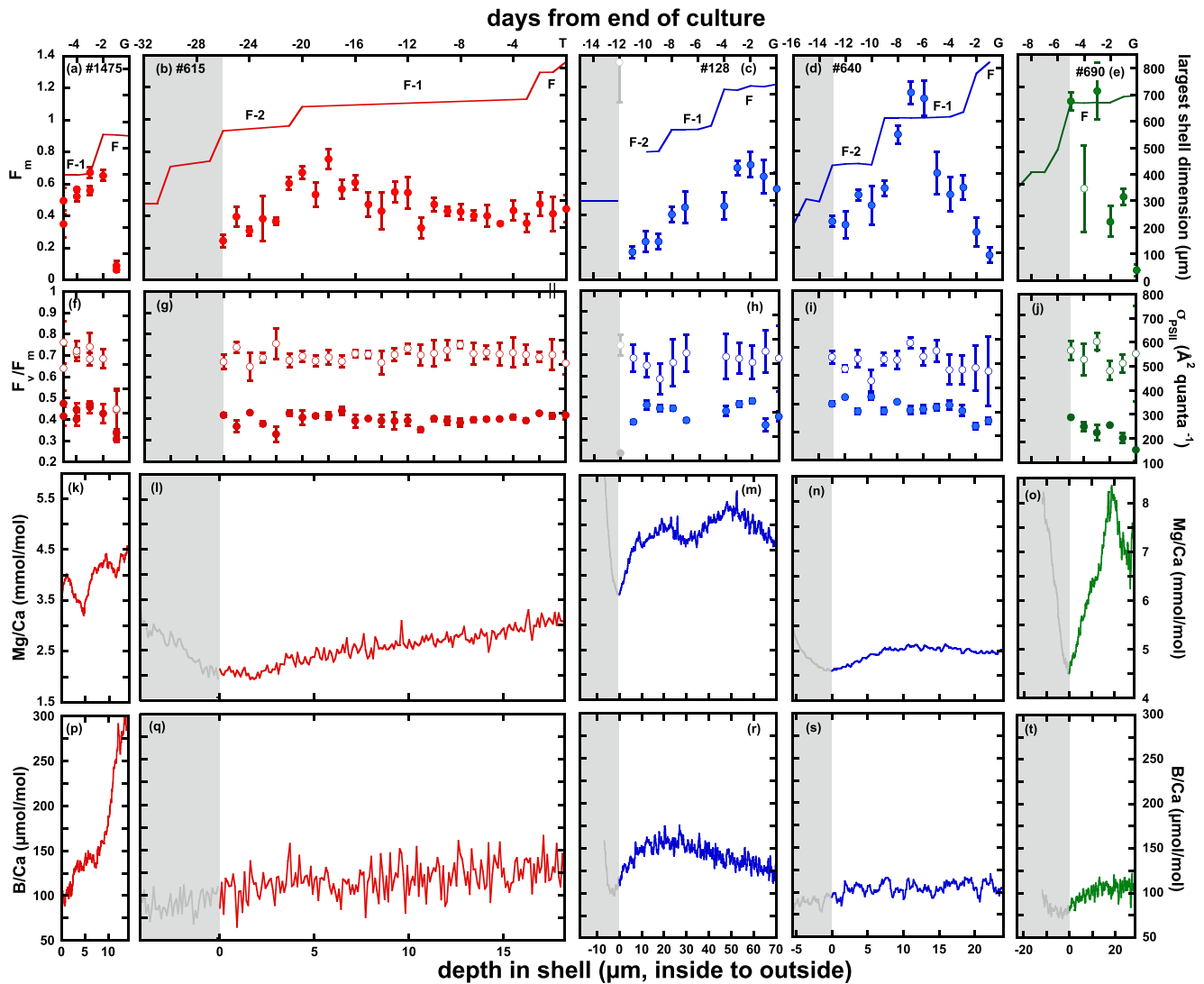
Figure 10. Fast rate repetition flourometry (FRRF) and laser ablation profiles of Mg/Ca and B/Ca measured on five *ontogenetic* specimens. The FRRF data are subsets from Figures 6 and 7; experimental specimen IDs are indicated in the top row of panels. Color-coding of foraminifer species is the same as in previous figures. Panels (a)–(e) show F_m data as solid symbols and shell growth as solid lines; the final (F), penultimate (F-1) and antepenultimate (F-2) chambers are labeled and can be identified by stepwise increases in maximum shell dimension. Panels (f)–(j) show F_v/F_m data as solid symbols and σ_{PSII} data as open symbols. Panels (k)–(o) display laser ablation profiles for Mg/Ca and (p)–(t) B/Ca. Note that the unusually high outer shell B/Ca data in panel (p) correlate with Al/Ca, indicating possible bias via interaction with the carbon tape the specimens were mounted on. The right-hand side Mg/Ca scale only applies to (o); *O. universa* incorporates more Mg than other species. Gray portions of each laser ablation profile display calcification inward from the primary organic sheet (POS), colored lines display the thicker calcification outward from the POS. Values of 0 on the lower abscissa mark the POS as identified by the minimum in Mg/Ca of each specimen's profile. Vertical alignment of the POS with the time (in days) of respective F-2, F-1, or F chamber formation of each specimen (see text for which chamber profile is presented for each specimen) allows quasi-temporal comparison of FRRF and corresponding laser ablation data collected over the same growth period. FRRF data that predate the portion of the shell observed by laser ablation have been eliminated.

specimens in the same size range. However, *G. ruber* rarely grows shells larger than 450 μm in maximum dimension, which is why paleoreconstructions based on fossil *G. ruber* specimens typically use the 250–355 μm shell size fraction. In contrast, adult *O. universa* grow a large spherical final chamber, and *T. sacculifer* specimens often secrete a large sac-like chamber before gametogenesis, so that the average maximum shell dimension of these three species in culture and in sediments generally decreases in the order *O. universa* > *T. sacculifer* > *G. ruber*. Symbiont abundance and Chl. *a* concentration of specimens observed herein follow that same order (Figure 3), with *O. universa* and *T. sacculifer* generally growing larger shells than *G. ruber* and larger shells are associated with greater symbiont abundances. Normalized to the foraminiferal cell's biomass (ng Chl. *a*/μg), Takagi et al. (2019) found *T. sacculifer* > *O. universa* > *G. ruber*. This species

ranking appears to contradict the hypothesis that the high B/Ca and δ^{11}B values recorded by *G. ruber* and *T. sacculifer* (Figure 1) could be caused by species-specific symbiont abundance and Chl. *a* concentration, which would instead predict Chl. *a*/biomass to decrease in the order *G. ruber* > *T. sacculifer* > *O. universa* to explain the observed boron proxy offsets (Figure 1).

As indicated in the introduction, the effect of symbiont-photosynthesis could be modulated by the photosynthesis/respiration ratio, where relatively greater respiration could reduce the pH elevation caused by photosynthesis. If the photosynthesis/respiration ratio is responsible for the geochemical effects shown in Figure 1, we would expect this ratio to decrease *G. ruber* > *T. sacculifer* > *O. universa*. Indeed, Lombard et al. (2009) observed greater respiration rates in *O. universa* than in *G. ruber*, but photosynthesis rates were also higher in *O. universa* (Figure S1), consistent with our and previous observations of greater symbiont abundance and Chl. *a* concentrations in *O. universa* (Figure 3). As shown in Figure S1, the photosynthesis/ respiration ratio is in fact the same for both *G. ruber* and *O. universa*, and lowest for *T. sacculifer* (Figure S1). Consequently, and although available data are limited, they do not allow us to explain the boron proxy offsets between the three species studied herein. A more systematic analysis of respiration is clearly warranted for planktic foraminifera, including on larger populations of individuals to overcome inter-specimen variability.

4.2. Symbiont Fluorescence Changes as Observed by FRRF

F_m is the most variable of the three FRRF parameters observed herein. In all three foraminifer species, F_m increased until ∼2–3 days prior to gametogenesis, followed by declining values toward gametogenesis (Figure 6). A few large specimens from the *ocean group* also displayed low F_m (Figure 5a), suggesting they may have been close to gametogenesis (Figure 5a). The observations of greater F_m (Figure 5a), symbiont abundance (Figure 3a), and Chl. *a* (Figure 3b) with shell size in the *ocean group* suggest that these three parameters are closely correlated. Given this evidence and the F_m/Chl. *a* correlations (Figure 4), we surmise that symbiont abundance and Chl. *a* content likely also increased in *ontogenetic specimens* as foraminifera grew in size, and then eventually decreased as specimens matured. F_v/F_m also tends to decline ∼2–3 days prior to gametogenesis (Figure 7) and is reduced in a few large specimens from the *ocean group* (Figure 5c). However, the F_v/F_m decline is less pronounced than in F_m, indicating that even as Chl. *a* concentrations declined toward gametogenesis, Chl. *a* remained functional and active photosynthesis took place (see similar discussion in Takagi et al., 2019), albeit at a lower rate. We suggest this *ontogenetic* decrease in F_m just prior to gametogenesis (Figure 6) is likely due to the symbiont population either being digested by the foraminifer (Bé et al., 1983) or expelled as live cells. Consistent with earlier studies, σ_{PSII} shows little variation throughout ontogeny (Figure 7 and Fujiki et al., 2014; Takagi et al., 2016), and between species (Figure 5 and Takagi et al., 2019). At most, the slight decline observed in a few of the largest specimens from the *ocean group* (Figure 5c) might suggest that those specimens were nearing gametogenesis, in which case their lower σ_{PSII} would be consistent with the idea of symbiont digestion or expulsion prior to gametogenesis.

In a few long-living *ontogenetic* specimens, the F_m decline occurred as early as 7–16 days prior to gametogenesis (Figures 6d, 6f, 7d and 7f). Visual inspection of the specimens at that time showed a change in the color of the symbionts from golden brown to gray, long before the foraminifers shortened their spines. Although this could be an indication that the symbionts were not healthy, F_v/F_m did not decrease until many days later (Figure 7), suggesting that Chl. *a* was still functional. We, therefore, assume that the color change may be more indicative of a decrease in symbiont abundance than symbiont photochemical quantum efficiency. This graying condition is observed rarely in culture but when it does occur, it can last for several days and is ultimately completed by gametogenesis similar to specimens that do not show this graying condition. Collectively, available evidence indicates F_m is the most variable FRRF parameter both through *ontogeny* (this study, Fujiki et al., 2014, 2016) and between planktic foraminifera species (this study, Takagi et al., 2019). The onset of the pre-gametogenic decrease in F_m is a consistent feature in all *ontogenetic* studies and could be used to predict the timing of the onset of gametogenesis in planktic foraminifers so that pre-gametogenic processes can be monitored more closely and the fate of symbionts before gametogenesis may ultimately be resolved.

4.3. Photosynthesis Effects on δ^{11}B and B/Ca Incorporation in Planktic Foraminifera Shells

Figure 8 explores possible δ^{11}B differences between HL and LL *O. universa* data that may have been caused by factors other than the light treatment. The data were all measured by N-TIMS and are internally consistent with the reference pH calibration lines shown in Figure 8, so the apparently elevated HL data point cannot be explained by differences in the analytical technique. However, while the LL sample was grown in Puerto Rico in 2015, the HL sample was cultured in 2010 as part of an N-TIMS/MC-ICP-MS analytical comparison with Bristol University. Analyzed with both techniques, the MC-ICP-MS results of the 3-point pH-calibration fell directly on the N-TIMS calibration of Sanyal et al. (1996) and Hönisch et al. (2009), whereas N-TIMS analysis of the same samples was elevated by 1.3‰ compared to the earlier studies (data reported in Hönisch et al., 2019). While the relative difference between the MC-ICP-MS and N-TIMS 2010 *O. universa* data is consistent with the known ~1–1.5‰ δ^{11}B offset between N-TIMS and MC-ICP-MS (see Text S1), the quantitative agreement between the MC-ICP-MS and the earlier N-TIMS calibrations (Hönisch et al., 2009; Sanyal et al., 1996) and the offset between the two sets of N-TIMS analyses is not. These comparisons suggest that the δ^{11}B value of *O. universa* cultured in Puerto Rico in 2010 is elevated above the earlier Catalina *O. universa* calibrations (Hönisch et al., 2009; Sanyal et al., 1996). Because the experimental and analytical procedures were identical between 2008 (i.e., the Catalina culture season used for the *O. universa* calibration data of Hönisch et al., 2009), and the 2010 and 2015 Puerto Rico culture seasons, Hönisch et al. (2019) speculated that a different genotype of *O. universa* with an elevated boron isotope composition may periodically dwell in the ocean off Puerto Rico. Furthermore, it is intriguing that our 2015 LL data point is consistent with a 1.87 ± 0.44‰ HL-LL δ^{11}B offset for this species when referenced to the HL data point of the original Catalina calibration. This smaller offset would bring *O. universa* in line with the offsets observed for *G. ruber* (2.02 ± 0.45‰) and *T. sacculifer* (1.95 ± 0.42‰), and with an earlier light experiment conducted with *O. universa* on Catalina that produced a 1.5 ± 0.67‰ HL-LL offset (Hönisch et al., 2003). While it is not possible to verify whether a different genotype dominated the *O. universa* population off Puerto Rico in 2010 than in 2015, we conclude that the δ^{11}B HL-LL offsets between all three species are either the same within error, or they are the same for *G. ruber* and *T. sacculifer* but higher for *O. universa* (Figure 8).

The Puerto Rico *O. universa* B/Ca data is shown in Figure 9 were all collected from samples grown during the same 2015 field season, so the problem discussed above with respect to δ^{11}B does not apply to B/Ca. Similar to δ^{11}B (Figure 8), B/Ca is elevated in HL experiments in *G. ruber* and Puerto Rico *O. universa*, but not in Catalina *O. universa* (Figure 9). The site-to-site and 2010/2015 variability in *O. universa* boron proxy responses complicates interpretation, but some of this may be explained by the low sensitivity of *O. universa* B/Ca ratios to pH (Figure 1). While bearing this caveat in mind, we will continue to use our data to test our hypothesis that differences in symbiont photosynthesis and light levels explain differences in boron incorporation (Figures 1 and 9). Specifically, because of the differential δ^{11}B and B/Ca systematics in the three foraminifer species studied herein (Figure 1), we hypothesized that HL-LL offsets in δ^{11}B and B/Ca, and by inference symbiont photosynthesis, should be largest in *G. ruber*, intermediate in *T. sacculifer*, and smallest in *O. universa*. In terms of B/Ca we note that whereas the decrease is larger in *absolute* values in *G. ruber* (pink, ΔB/Ca = 26 μmol/mol) than in *O. universa* (ΔB/Ca$_{PR}$ = 8 μmol/mol), *G. ruber* (pink) incorporates generally more boron than *O. universa* (Figures 1 and 9), and the *relative* B/Ca decrease between HL and LL experiments is similar for *G. ruber* (pink) and Puerto Rico *O. universa* (18.4% and 17.2%, respectively). In summary, symbiont photosynthesis raises δ^{11}B in all three species (Figure 8) and B/Ca at least in *G. ruber* and in some *O. universa* (Figure 9).

For δ^{11}B we can conclude the symbiont effect is not larger in *G. ruber* (pink) than in the other two species and photosynthesis alone therefore cannot explain the species-specific offsets in culture and coretop calibrations. The HL-LL offsets in B/Ca agree with our hypothesis when considering only *G. ruber* (pink) and Catalina *O. universa*, but the offsets are inconsistent with the hypothesis when comparing *G. ruber* (pink) and Puerto Rico *O. universa*. In fact, the proportional HL-LL decrease in Puerto Rico *O. universa* and *G. ruber* (pink) B/Ca may be another indication that the symbiont effect is the same in both species, at least for this culture location. Because controls on the B/Ca proxy are complex (Allen & Hönisch, 2012; Allen et al., 2012; Haynes et al., 2019) and because B/Ca in *O. universa* is less sensitive to marine carbonate chemistry than in *G. ruber* and *T. sacculifer* (Figure 1), we place greater weight on the inferences from the δ^{11}B proxy, which does not support our hypothesis. Following this line of argument, and because species-specific

δ^{11}B and B/Ca offsets are the same in both laboratory-grown (Figures 1 and 8) and ocean-grown (i.e., sediment coretop) samples (for a compilation of coretop data see Henehan et al., 2016; Hönisch et al., 2019), we conclude that symbiont photosynthesis elevates δ^{11}B and probably also B/Ca in planktic foraminifera. However, symbiont photosynthesis does not explain species-specific offsets in boron proxy geochemistry, which requires additional information on respiration and/or biomineralization.

Our inferences from the light experiments performed for boron geochemistry are further supported by our FRRF data, which also contradict the hypothesis of greater symbiont photochemical quantum efficiency in *G. ruber* > *T. sacculifer* > *O. universa*. The *ocean groups* of the three foraminifera species display a clear pattern of more symbionts (Figure 3a) and higher Chl. *a* content with increasing specimen size (Figure 3b), but there is no significant inter-species difference in these parameters other than *G. ruber* specimens being generally smaller than *T. sacculifer* and *O. universa* (Figure 3). These shell sizes are typical for these species and are similar to their fossil representation in the sediment. As Chl. *a* is the primary pigment used to collect light energy for photosynthesis, and Chl. *a* is more abundant in larger specimens (Figure 3b), we predicted greater symbiont photochemical quantum efficiency in the largest specimens, at least before the onset of gametogenesis. This prediction is partly confirmed by slightly greater F_m in *O. universa* specimens than in *G. ruber* and *T. sacculifer*, which display similar values (Figure 5a) across all size ranges. For *G. ruber* in particular, this species may hold its symbionts closer to its shell surface (Figure S2b), resulting in symbionts shading each other and therefore lower F_m. While we do not have the data needed to test symbiont shading, these results collectively contradict our photosynthesis hypothesis on boron incorporation, as they suggest the greatest photosynthetic activity in *O. universa* > *T. sacculifer* > *G. ruber*. As discussed above, photochemical quantum efficiencies (F_v/F_m, Figure 5b) and functional absorption cross sections of photosystem II (σ_{PSII}, Figure 5c) are essentially the same for all three species, a result that is not surprising given that all three species harbor the same species of dinoflagellate symbionts, and that dinoflagellate-bearing foraminifera species have generally been found to vary little in both F_v/F_m and σ_{PSII} (Takagi et al., 2019).

As alluded to, the symbiont density (i.e., how tight each foraminifer species holds its symbiont population near the shell surface, see Figure S1 for pictures of live specimens with variable symbiont spreading) or the symbiont-to-cytoplasm ratio could still differ significantly between species. Studying those parameters would require (a) observation of symbiont spreading around the shell and FRRF parameters throughout the day and (b) more rigorous quantification of the cytoplasm volume of foraminifera with different shapes, sizes and chamber fill. This would require more intensive observational data than we currently have and could be the subject of future studies. Normalizing symbiont photochemical quantum efficiency to microenvironment volume, accounting for symbiont positioning, and simultaneously monitoring photosynthetic oxygen evolution and symbiont-host respiration will likely provide additional insight into the potential influence of symbiont activity on boron incorporation.

The laser ablation profiles were analyzed to test whether at least the *ontogenetic* trends in symbiont photosynthetic activity correlate with the geochemical signals recorded by the same specimens. Mg/Ca is a well-established temperature proxy (e.g., Anand et al., 2003) but laser ablation studies have identified daily banding in Mg/Ca, where higher Mg/Ca ratios are incorporated at night (Spero et al., 2015). As such, we would expect to see opposite banding patterns in Mg/Ca and B/Ca if light were the dominant parameter controlling ontogenetic variations in these element ratios, but B/Ca banding in our Puerto Rico specimens (Figure 10) is not very pronounced.

Assuming that greater F_m reflects overall higher symbiont biomass in the symbiont-host associations, our ontogenetic F_m trends (Figures 6 and 9a–9e) would suggest B/Ca should increase as the foraminifer ages and chamber walls thicken and decrease just prior to gametogenesis as F_m decreases. We do find that B/Ca is typically elevated outward from the POS (Figure 10, and also Allen et al., 2011; Holland et al., 2017), but B/Ca maxima are typically reached halfway through the chamber wall; at least one *T. sacculifer* specimen (Figure 10r) displays a significant decrease in B/Ca toward the outer shell surface. Given the temporal alignment of FRRF and trace element data may not be perfect, the increase in B/Ca away from the POS may be related to the increased photosynthesis observed through *ontogeny*. However, the pre-gametogenic decrease in F_m is not or at least not consistently reflected in B/Ca, and there is no clear scaling between F_m and B/Ca across these five specimens (see Section 3.6 and Figures 4 and 10). Following our species-specific boron

proxy incorporation hypothesis, we would have expected F_m to scale with B/Ca in the order *G. ruber* > *T. sacculifer* > *O. universa*, but this pattern is not evident in the five specimens studied herein.

4.4. Could Accounting for Respiration and/or Biomineralization Explain Our Observations?

Symbiont photosynthesis is only one of several physiological processes influencing the foraminiferal microenvironment. For instance, respiration and the calcification process itself produce CO_2 and thereby lower pH in the foraminiferal microenvironment (Jørgensen et al., 1985; Köhler-Rink & Kühl, 2005; Rink et al., 1998). If different foraminifer species respire and/or calcify at different rates, this may lead to variations in pH. Respiration rates have been inferred from microelectrode O_2 measurements in the dark (Jørgensen et al., 1985; Köhler-Rink & Kühl, 2005; Lombard et al., 2009; Rink et al., 1998), but to date, very few data have been collected systematically under the same physicochemical conditions across species and size ranges (Figure S1). Evidence from these data is intriguing but not yet conclusive and more work is needed to corroborate the preliminary findings.

In terms of calcification, *G. ruber* secretes thinner shell walls than *T. sacculifer* and *O. universa*, but it does so over a semi-lunar rather than a lunar cycle (Schiebel & Hemleben, 2017) and therefore may calcify faster than either *T. sacculifer* or *O. universa*, at least during ontogeny. However, *T. sacculifer* and *O. universa* also secrete gametogenic calcite in a rapid final calcification event, and overall (i.e., ontogenetic through gametogenetic) calcification rates have been estimated to follow the order *O. universa* > *T. sacculifer* > *G. ruber* (Allen et al., 2016). Shell thickening estimated from laser ablation pulses is shown in Figure 10 (where *T. sacculifer* and *O. universa* specimens grew thicker chambers than *G. ruber* (pink) specimens), but estimating calcification rates from these data is difficult without time constraints. However, the similarity of the HL-LL boron proxy differences between the three species (Figures 8 and 9 and Hönisch et al., 2003) seems to contradict the idea that simple calcification rate effects could explain the overall geochemical offsets between these three foraminifera species.

Finally, species-specific differences in the timing or mechanism of the biomineralization process, for example, differences in day/night calcification, ion channeling or ion pumping (for a review, see de Nooijer et al., 2014), and consequent differences in boron discrimination from the calcifying fluid could cause the observed geochemical offsets (see also Haynes et al., 2019). For instance, based on ^{45}Ca uptake experiments, it has been estimated that *O. universa* secretes 30% of its shell at night (Lea et al., 1995), or roughly 50% based on day/night barium labeling (Vetter et al., 2013). Similar experiments have not yet been performed for *T. sacculifer* or *G. ruber*, not to mention inter-specimen variability, but if these species produce a relatively greater proportion of their shell during the day (e.g., 60% day-time calcification for *T. sacculifer* and 90% for *G. ruber*) then that could produce sufficiently elevated bulk shell B/Ca values to explain the species differences. Testing this hypothesis will require dedicated experiments to determine the day/night calcification proportions in the different species.

5. Conclusions

The observation of elevated bulk shell $\delta^{11}B$ and B/Ca of planktic symbiont-bearing foraminifera grown in HL conditions in addition to higher F_m and elevated B/Ca within the shell walls of individual specimens support the notion that symbiont photosynthesis causes at least some pH-elevation in the calcifying microenvironment and/or exerts some influence on boron incorporation into symbiont-bearing planktic foraminifera shells. However, the light effect on boron proxies is rather uniform among the three species studied herein and by itself cannot explain the species-specific offsets in absolute B/Ca and $\delta^{11}B$.

With the experimental data available to date, we cannot ascribe the boron proxy offsets among the three foraminifer species studied herein to differences in symbiont photosynthesis, and we are currently unable to identify the root cause of these offsets. This outcome raises concerns about inferring the prevalence and magnitude of physiological pH elevation from fossils and from geochemical proxies that are themselves understood incompletely. Further work on the mechanisms of foraminiferal biomineralization and their influence on B incorporation is required to determine the precise origin of inter-species vital effects on boron-based proxies.

Data Availability Statement

Analytical data are accessible electronically in the Data Supplement and at https://www.ncdc.noaa.gov/paleo/study/23151.

References

Allen, K. A., & Hönisch, B. (2012). The planktic foraminiferal B/Ca proxy for seawater carbonate chemistry: A critical evaluation. *Earth and Planetary Science Letters*, *345–348*, 203–211. https://doi.org/10.1016/j.epsl.2012.06.012

Allen, K. A., Hönisch, B., Eggins, S. M., Haynes, L. L., Rosenthal, Y., & Yu, J. (2016). Trace element proxies for surface ocean conditions: A synthesis of culture calibrations with planktic foraminifera. *Geochimica et Cosmochimica Acta*, *193*, 197–221. https://doi.org/10.1016/j.gca.2016.08.015

Allen, K. A., Hönisch, B., Eggins, S. M., & Rosenthal, Y. (2012). Environmental controls on B/Ca in calcite tests of the tropical planktic foraminifer species *Globigerinoides ruber* and *Globigerinoides sacculifer*. *Earth and Planetary Science Letters*, *351–352*, 270–280. https://doi.org/10.1016/j.epsl.2012.07.004

Allen, K. A., Hönisch, B., Eggins, S. M., Yu, J. M., Spero, H. J., & Elderfield, H. (2011). Controls on boron incorporation in cultured tests of the planktic foraminifer *Orbulina universa*. *Earth and Planetary Science Letters*, *309*, 291–301. https://doi.org/10.1016/j.epsl.2011.07.010

Anand, P., Elderfield, H., & Conte, M. H. (2003). Calibration of Mg/Ca thermometry in planktonic foraminifera from a sediment trap time series. *Paleoceanography*, *18*, 15. https://doi.org/10.1029/2002pa000846

Arbuszewski, J., deMenocal, P., Kaplan, A., & Farmer, E. C. (2010). On the fidelity of shell-derived $\delta^{18}O_{seawater}$ estimates. *Earth and Planetary Science Letters*, *300*, 185–196. https://doi.org/10.1016/j.epsl.2010.10.035

Babila, T. L., Rosenthal, Y., & Conte, M. H. (2014). Evaluation of the biogeochemical controls on B/Ca of *Globigerinoides ruber* white from the oceanic flux program, Bermuda. *Earth and Planetary Science Letters*, *404*, 67–76. https://doi.org/10.1016/j.epsl.2014.05.053

Bé, A. W. H., Anderson, O. R., Faber, W. W., Jr, Caron, D. A., & Be, A. W. H. (1983). Sequence of morphological and cytoplasmic changes during gametogenesis in the planktonic foraminifer Globigerinoides sacculifer (Brady). *Micropaleontology*, *29*, 310–325. https://doi.org/10.2307/1485737

Bé, A. W. H., Spero, H. J., & Anderson, O. R. (1982). Effects of symbiont elimination and reinfection on the life processes of the planktonic foraminifer *Globigerinoides sacculifer*. *Marine Biology*, *70*, 73–86.

Bentov, S., Brownlee, C., & Erez, J. (2009). The role of seawater endocytosis in the biomineralization process in calcareous foraminifera. *Proceedings of the National Academy of Sciences*, *106*, 21500–21504. https://doi.org/10.1073/pnas.0906636106

Caron, D. A., Bé, A. W. H., & Anderson, O. R. (1981). Effects of variations in light intensity on life processes of the planktonic foraminifer *Globigerinoides sacculifer* in laboratory culture. *Journal of the Marine Biological Association of the United Kingdom*, *62*, 435–451.

de Nooijer, L. J., Spero, H. J., Erez, J., Bijma, J., & Reichart, G. J. (2014). Biomineralization in perforate foraminifera. *Earth-Science Reviews*, *135*, 48–58. https://doi.org/10.1016/j.earscirev.2014.03.013

Dickson, A. G. (1990a). Standard potential of the reaction: AgCl(s) + 1/2H$_2$(g) = Ag(s) + HCl(aq), and the standard acidity constant of the ion HSO$_4^-$ in synthetic seawater from 273.15 to 318.15 K. *Journal of Chemical Thermodynamics*, *22*, 113–127. https://doi.org/10.1016/0021-9614(90)90074-z

Dickson, A. G. (1990b). Thermodynamics of the dissociation of boric acid in synthetic seawater from 273.15 to 318.15 K. *Deep-Sea Research*, *37*, 755–766. https://doi.org/10.1016/0198-0149(90)90004-f

Dyez, K. A., Hönisch, B., & Schmidt, G. A. (2018). Early pleistocene obliquity-scale pCO$_2$ variability at ~1.5 million years ago. *Paleoceanography and Paleoclimatology*, *33*. https://doi.org/10.1029/2018pa003349

Eggins, S., De Deckker, P., & Marshall, J. (2003). Mg/Ca variation in planktonic foraminifera tests: Implications for reconstructing palaeo-seawater temperature and habitat migration. *Earth and Planetary Science Letters*, *212*, 291–306. https://doi.org/10.1016/s0012-821x(03)00283-8

Eggins, S. M., Sadekov, A., & De Deckker, P. (2004). Modulation and daily banding of Mg/Ca in Orbulina universa tests by symbiont photosynthesis and respiration: A complication for seawater thermometry? *Earth and Planetary Science Letters*, *225*, 411–419. https://doi.org/10.1016/j.epsl.2004.06.019

Erez, J. (2003). The source of ions for biomineralization in foraminifera and their implications for paleoceanographic proxies. *Reviews in Mineralogy and Geochemistry*, *54*, 115–150. https://doi.org/10.1515/9781501509346-010

Falkowski, P. G., Koblizek, M., Gorbunov, M., & Kolber, Z. (2004). Development and application of variable chlorophyll fluorescence techniques in marine ecosystems. In G. C. Pageorigiou, & R. Govindjee (Eds.), *Chlorophyll a fluorescence: A signature of photosynthesis* (pp. 757–778). Springer.

Foster, G. L. (2008). Seawater pH, pCO$_2$ and [CO$_3^{2-}$] variations in the Caribbean Sea over the last 130 kyr: A boron isotope and B/Ca study of planktic foraminifera. *Earth and Planetary Science Letters*, *271*, 254–266. https://doi.org/10.1016/j.epsl.2008.04.015

Foster, G. L., Hönisch, B., Paris, G., Dwyer, G. S., Rae, J. W. B., Elliott, T., et al. (2013). Interlaboratory comparison of boron isotope analyses of boric acid, seawater and marine CaCO$_3$ by MC-ICPMS and NTIMS. *Chemical Geology*, *358*, 1–14. https://doi.org/10.1016/j.chemgeo.2013.08.027

Fujiki, T., Takagi, H., Kimoto, K., Kurasawa, A., Yuasa, T., & Mino, Y. (2014). Assessment of algal photosynthesis in planktic foraminifers by fast repetition rate fluorometry. *Journal of Plankton Research*, *36*, 1403–1407. https://doi.org/10.1093/plankt/fbu083

Haynes, L. L., Hönisch, B., Dyez, K. A., Holland, K., Rosenthal, Y., Fish, C. R., et al. (2017). Calibration of the B/Ca proxy in the planktic foraminifer *Orbulina universa* to paleocene seawater conditions. *Paleoceanography*, *32*, 580–599. https://doi.org/10.1002/2016pa003069

Haynes, L. L., Hönisch, B., Holland, K., Rosenthal, Y., & Eggins, S. M. (2019). Evaluating the planktic foraminiferal B/Ca proxy for application to deep time paleoceanography. *Earth and Planetary Science Letters*, *528*, 115824. https://doi.org/10.1016/j.epsl.2019.115824

Hemming, N. G., & Hanson, G. N. (1992). Boron isotopic composition and concentration in modern marine carbonates. *Geochimica et Cosmochimica Acta*, *56*, 537–543. https://doi.org/10.1016/0016-7037(92)90151-8

Henehan, M. J., Foster, G. L., Bostock, H. C., Greenop, R., Marshall, B. J., & Wilson, P. A. (2016). A new boron isotope-pH calibration for *Orbulina universa*, with implications for understanding and accounting for "vital effects". *Earth and Planetary Science Letters*, *454*, 282–292. https://doi.org/10.1016/j.epsl.2016.09.024

Henehan, M. J., Rae, J. W. B., Foster, G. L., Erez, J., Prentice, K. C., Kucera, M., et al. (2013). Calibration of the boron isotope proxy in the planktonic foraminifera *Globigerinoides ruber* for use in palaeo-CO$_2$ reconstruction. *Earth and Planetary Science Letters*, *364*, 111–122. https://doi.org/10.1016/j.epsl.2012.12.029

Holland, K., Eggins, S. M., Hönisch, B., Haynes, L. L., & Branson, O. (2017). Calcification rate and shell chemistry response of the planktic foraminifer *Orbulina universa* to changes in microenvironment seawater carbonate chemistry. *Earth and Planetary Science Letters*, *464*, 124–134. https://doi.org/10.1016/j.epsl.2017.02.018

Holm-Hansen, O., & Riemann, B. (1978). Chlorophyll a determination: Improvements in methodology. *Oikos*, *30*, 438–447. https://doi.org/10.2307/3543338

Hönisch, B., Bijma, J., Russell, A. D., Spero, H. J., Palmer, M. R., Zeebe, R. E., & Eisenhauer, A. (2003). The influence of symbiont photosynthesis on the boron isotopic composition of foraminifera shells. *Marine Micropaleontology*, *49*, 87–96. https://doi.org/10.1016/s0377-8398(03)00030-6

Hönisch, B., Eggins, S. M., Haynes, L. L., Allen, K. A., Holland, K., & Lorbacher, K. (2019). *Boron proxies in Paleoceanography and Paleoclimatology*. John Wiley & Sons, Ltd.

Hönisch, B., & Hemming, N. G. (2004). Ground-truthing the boron isotope paleo-pH proxy in planktonic foraminifera shells: Partial dissolution and shell size effects. *Paleoceanography*, *19*. https://doi.org/10.1029/2004PA001026

Hönisch, B., Hemming, N. G., Archer, D., Siddall, M., & McManus, J. F. (2009). Atmospheric carbon dioxide concentration across the mid-Pleistocene transition. *Science*, *324*, 1551–1554. https://doi.org/10.1126/science.1171477

JGOFS-protocols. (1996). *Protocols for the joint global ocean flux study (JGOFS) core measurements*.

Jørgensen, B. B., Erez, J., Revsbech, N. P., & Cohen, Y. (1985). Symbiotic photosynthesis in a planktonic foraminiferan, *Globigerinoides sacculifer* (Brady), studied with microelectrodes. *Limnology & Oceanography*, *30*, 1253–1267.

Klochko, K., Kaufman, A. J., Yao, W., Byrne, R. H., & Tossell, J. A. (2006). Experimental measurement of boron isotope fractionation in seawater. *Earth and Planetary Science Letters*, *248*, 261–270. https://doi.org/10.1016/j.epsl.2006.05.034

Köhler-Rink, S., & Kühl, M. (2005). The chemical microenvironment of the symbiotic planktonic foraminifer *Orbulina universa*. *Marine Biology Research*, *1*, 68–78. https://doi.org/10.1080/17451000510019015

Kolber, Z. S., Prášil, O., & Falkowski, P. G. (1998). Measurements of variable chlorophyll fluorescence using fast repetition rate techniques: Defining methodology and experimental protocols. *Biochimica et Biophysica Acta*, *1367*, 88–106. https://doi.org/10.1016/s0005-2728(98)00135-2

Lea, D. W., Martin, P. A., Chan, D. A., & Spero, H. J. (1995). Calcium uptake and calcification rate in the planktonic foraminifer *Orbulina universa*. *Journal of Foraminiferal Research*, *25*, 14–23. https://doi.org/10.2113/gsjfr.25.1.14

Lee, K., Kim, T.-W., Byrne, R. H., Millero, F. J., Feely, R. A., & Liu, Y.-M. (2010). The universal ratio of boron to chlorinity for the North Pacific and North Atlantic oceans. *Geochimica et Cosmochimica Acta*, *74*, 1801–1811. https://doi.org/10.1016/j.gca.2009.12.027

Lombard, F., Erez, J., Michel, E., & Labeyrie, L. (2009). Temperature effect on respiration and photosynthesis of the symbiont-bearing planktonic foraminifera *Globigerinoides ruber*, *Orbulina universa*, and *Globigerinella siphonifera*. *Limnology & Oceanography*, *54*, 210–218. https://doi.org/10.4319/lo.2009.54.1.0210

Longerich, H. P., Jackson, S. E., & Günther, D. (1996). Inter-laboratory note. Laser ablation inductively coupled plasma mass spectrometric transient signal data acquisition and analyte concentration calculation. *Journal of Analytical Atomic Spectrometry*, *11*, 899–904. https://doi.org/10.1039/ja9961100899

Lueker, T. J., Dickson, A. G., & Keeling, C. D. (2000). Ocean pCO$_2$ calculated from dissolved inorganic carbon, alkalinity, and equations for K1 and K2: Validation based on laboratory measurements of CO$_2$ in gas and seawater at equilibrium. *Marine Chemistry*, *70*, 105–119. https://doi.org/10.1016/s0304-4203(00)00022-0

Martínez-Botí, M. A., Foster, G. L., Chalk, T. B., Rohling, E. J., Sexton, P. F., Lunt, D. J., et al. (2015). Plio-Pleistocene climate sensitivity evaluated using high-resolution CO$_2$ records. *Nature*, *518*, 49–54. https://doi.org/10.1038/nature14145

Osborne, E. B., Umling, N. E., Bizimis, M., Buckley, W., Sadekov, A., Tappa, E., et al. (2020). A sediment trap evaluation of B/Ca as a carbonate system proxy in asymbiotic and nondinoflagellate hosting planktonic foraminifera. *Paleoceanography and Paleoclimatology*, *35*, e2019PA003682. https://doi.org/10.1029/2019pa003682

Paillard, D., Labeyrie, L., & Yiou, P. (1996). Macintosh program performs time-series analysis. *Eos, Transactions American Geophysical Union*, *77*, 379–379. https://doi.org/10.1029/96eo00259

Pierrot, D., Lewis, E., & Wallace, D. W. R. (2006). *MS excel program developed for CO2 system calculations*. Carbon Dioxide Information Analysis Center, Oak Ridge National Laboratory, US Department of Energy.

Rink, S., Kühl, M., Bijma, J., & Spero, H. J. (1998). Microsensor studies of photosynthesis and respiration in the symbiotic foraminifer *Orbulina universa*. *Marine Biology*, *131*, 583–595. https://doi.org/10.1007/s002270050350

Rosenthal, Y., Field, M. P., & Sherrell, R. M. (1999). Precise determination of element/calcium ratios in calcareous samples using sector field inductively coupled plasma mass spectrometry. *Analytical Chemistry*, *71*, 3248–3253. https://doi.org/10.1021/ac981410x

Russell, A. D., Hönisch, B., Spero, H. J., & Lea, D. W. (2004). Effects of changes in seawater carbonate ion concentration and temperature on shell U/Ca, Mg/Ca, and Sr/Ca of planktonic foraminifera. *Geochimca Cosmochimica Acta*, *68*, 4347–4361. https://doi.org/10.1016/j.gca.2004.03.013

Sadekov, A. Y., Eggins, S. M., & De Deckker, P. (2005). Characterization of Mg/Ca distributions in planktonic foraminifera species by electron microprobe mapping. *Geochemistry, Geophysics and Geosystems*, *6*. https://doi.org/10.1029/2005gc000973

Sanyal, A., Bijma, J., Spero, H. J., & Lea, D. W. (2001). Empirical relationship between pH and the boron isotopic composition of *Globigerinoides sacculifer*: Implications for the boron isotope paleo-pH proxy. *Paleoceanography*, *16*, 515–519. https://doi.org/10.1029/2000pa000547

Sanyal, A., Hemming, N. G., Broecker, W. S., Lea, D. W., Spero, H. J., & Hanson, G. N. (1996). Oceanic pH control on the boron isotopic composition of foraminifera: Evidence from culture experiments. *Paleoceanography*, *11*, 513–517. https://doi.org/10.1029/96pa01858

Schiebel, R., & Hemleben, C. (2017). *Planktic foraminifers in the modern ocean* (2nd ed.): Springer-Verlag.

Seki, O., Foster, G. L., Schmidt, D. N., Mackensen, A., Kawamura, K., & Pancost, R. D. (2010). Alkenone and boron-based Pliocene pCO$_2$ records. *Earth and Planetary Science Letters*, *292*, 201–211. https://doi.org/10.1016/j.epsl.2010.01.037

Shaked, Y., & de Vargas, C. (2006). Pelagic photosymbiosis: rDNA assessment of diversity and evolution of dinoflagellate symbionts and planktonic foraminiferal hosts. *Marine Ecology Progress Series*, *325*, 59–71. https://doi.org/10.3354/meps325059

Siano, R., Montresor, M., Probert, I., Not, F., & de Vargas, C. (2010). Pelagodinium gen. nov. and P. béii comb. nov., a dinoflagellate Symbiont of Planktonic Foraminifera. *Protist*, *161*, 385–399. https://doi.org/10.1016/j.protis.2010.01.002

Spero, H. J. (1987). Symbiosis in the planktonic foraminifer, *Orbulina universa*, and the isolation of its symbiotic dinoflagellate, *Gymnodinium béii* sp. nov. *Journal of Phycology*, *23*, 307–317. https://doi.org/10.1111/j.1529-8817.1987.tb04139.x

Spero, H. J., Eggins, S. M., Russell, A. D., Vetter, L., Kilburn, M. R., & Hönisch, B. (2015). Timing and mechanism for intratest Mg/Ca variability in a living planktic foraminifer. *Earth and Planetary Science Letters*, *409*, 32–42. https://doi.org/10.1016/j.epsl.2014.10.030

Spero, H. J., & Lea, D. W. (1993). Intraspecific stable isotope variability in the planktic foraminifera *Globigerinoides sacculifer*: Results from laboratory experiments. *Marine Micropaleontology*, *22*, 221–234. https://doi.org/10.1016/0377-8398(93)90045-y

Spero, H. J., & Parker, S. L. (1985). Photosynthesis in the symbiotic planktonic foraminifer *Orbulina universa*, and its potential contribution to oceanic primary productivity. *Journal of Foraminiferal Research*, *15*, 273–281. https://doi.org/10.2113/gsjfr.15.4.273

Takagi, H., Kimoto, K., Fujiki, T., Kurasawa, A., Moriya, K., & Hirano, H. (2016). Ontogenetic dynamics of photosymbiosis in cultured planktic foraminifers revealed by fast repetition rate fluorometry. *Marine Micropaleontology*, *122*, 44–52. https://doi.org/10.1016/j.marmicro.2015.10.003

Takagi, H., Kimoto, K., Fujiki, T., Saito, H., Schmidt, C., Kucera, M., & Moriya, K. (2019). Characterizing photosymbiosis in modern planktonic foraminifera. *Biogeosciences*, *16*, 3377–3396. https://doi.org/10.5194/bg-16-3377-2019

Vengosh, A., Kolodny, Y., Starinsky, A., Chivas, A. R., & McCulloch, M. T. (1991). Coprecipitation and isotopic fractionation of boron in modern biogenic carbonates. *Geochimica et Cosmochimica Acta*, *55*, 2901–2910. https://doi.org/10.1016/0016-7037(91)90455-e

Vetter, L., Kozdon, R., Mora, C. I., Eggins, S. M., Valley, J. W., Hönisch, B., & Spero, H. J. (2013). Micron-scale intrashell oxygen isotope variation in cultured planktic foraminifers. *Geochimica et Cosmochimica Acta*, *107*, 267–278. https://doi.org/10.1016/j.gca.2012.12.046

Yu, J., Elderfield, H., & Hönisch, B. (2007). B/Ca in planktonic foraminifera as a proxy for surface seawater pH. *Paleoceanography*, *22*. https://doi.org/10.1029/2006pa001347

Yu, J., Thornalley, D. J. R., Rae, J. W. B., & McCave, N. I. (2013). Calibration and application of B/Ca, Cd/Ca, and δ^{11}B in *Neogloboquadrina pachyderma* (sinistral) to constrain CO_2 uptake in the subpolar North Atlantic during the last deglaciation. *Paleoceanography*. *28* (2).

Zeebe, R. E., Wolf-Gladrow, D. A., Bijma, J., & Hönisch, B. (2003). Vital effects in foraminifera do not compromise the use of δ^{11}B as a paleo-pH indicator: Evidence from modeling. *Paleoceanography*, *18*, 1–9. https://doi.org/10.1029/2003pa000881